HHS Public Access

Author manuscript

*Pharmacol Res*. Author manuscript; available in PMC 2017 November 01.

Published in final edited form as:

*Pharmacol Res*. 2016 November ; 113(Pt A): 18–37. doi:10.1016/j.phrs.2016.08.016.

# Screening of a composite library of clinically used drugs and well-characterized pharmacological compounds for cystathionine β-synthase inhibition identifies benserazide as a drug potentially suitable for repurposing for the experimental therapy of colon cancer

**Nadiya Druzhyna**[a], **Bartosz Szczesny**[a], **Gabor Olah**[a], **Katalin Módis**[a,b], **Antonia Asimakopoulou**[c,d], **Athanasia Pavlidou**[e], **Petra Szoleczky**[a], **Domokos Gerö**[a], **Kazunori Yanagi**[a], **Gabor Törö**[a], **Isabel López-García**[a], **Vassilios Myrianthopoulos**[e], **Emmanuel Mikros**[e], **John R. Zatarain**[b], **Celia Chao**[b], **Andreas Papapetropoulos**[d,e], **Mark R. Hellmich**[b,f], and **Csaba Szabo**[a,f,*]

[a]Department of Anesthesiology, The University of Texas Medical Branch, Galveston, TX, USA

[b]Department of Surgery, The University of Texas Medical Branch, Galveston, TX, USA

[c]Laboratory of Molecular Pharmacology, Department of Pharmacy, University of Patras, Greece

[d]Center of Clinical, Experimental Surgery & Translational Research, Biomedical Research Foundation of the Academy of Athens, Greece

[e]National and Kapodistrian University of Athens, School of Pharmacy, Athens, Greece

[f]CBS Therapeutics Inc., Galveston, TX, USA

## Abstract

Cystathionine-β-synthase (CBS) has been recently identified as a drug target for several forms of cancer. Currently no potent and selective CBS inhibitors are available. Using a composite collection of 8871 clinically used drugs and well-annotated pharmacological compounds (including the LOPAC library, the FDA Approved Drug Library, the NIH Clinical Collection, the New Prestwick Chemical Library, the US Drug Collection, the International Drug Collection, the `Killer Plates' collection and a small custom collection of PLP-dependent enzyme inhibitors), we conducted an *in vitro* screen in order to identify inhibitors for CBS using a primary 7-azido-4-methylcoumarin (AzMc) screen to detect CBS-derived hydrogen sulfide ($H_2S$) production. Initial hits were subjected to counterscreens using the methylene blue assay (a secondary assay to

[*]Corresponding author at: Department of Anesthesiology, The University of Texas Medical Branch, 601 Harborside Drive, Building 21, Room 4.202D, Galveston, TX 77555-1102, USA. szabocsaba@aol.com (C. Szabo).

**Competing interests** C.C., A.P., M.H. and C.S are shareholders and/or officers of CBS Therapeutics Inc., a UTMB spin-off company involved in research and development of CBS inhibitors for the therapy of cancer. The other authors declare no conflicts of interest in relationship to this study.

**Authors' contributions** Nadiya Druzhyna: conduction of experiments, analysis of data, preparation of manuscript; Gabor Olah, Bartosz Szczesny, Katalin Módis, Antonia Asimakopoulou, Athanasia Pavlidou, Petra Szoleczky, Domokos Gerö, Gabor Törö, Isabel Lopez-Garcia, Vassilios Myrianthopoulos, John R. Zatarain, Celia Chao and Emmanuel Mikros: conduction of experiments, analysis of data, Andreas Papapetropoulos, Mark R. Hellmich and Csaba Szabo: experimental design, interpretation of the data, preparation of manuscript.

measure $H_2S$ production) and were assessed for their ability to quench the $H_2S$ signal produced by the $H_2S$ donor compound GYY4137. Four compounds, hexachlorophene, tannic acid, aurintricarboxylic acid and benserazide showed concentration-dependent CBS inhibitory actions without scavenging $H_2S$ released from GYY4137, identifying them as direct CBS inhibitors. Hexachlorophene ($IC_{50}$: ~60 μM), tannic acid ($IC_{50}$: ~40 μM) and benserazide ($IC_{50}$: ~30 μM) were less potent CBS inhibitors than the two reference compounds AOAA ($IC_{50}$: ~3 μM) and NSC67078 ($IC_{50}$: ~1 μM), while aurintricarboxylic acid ($IC_{50}$: ~3 μM) was equipotent with AOAA. The second reference compound NSC67078 not only inhibited the CBS-induced AzMC fluorescence signal ($IC_{50}$: ~1 μM), but also inhibited with the GYY4137-induced AzMC fluorescence signal with ($IC_{50}$ of ~6 μM) indicative of scavenging/non-specific effects. Hexachlorophene ($IC_{50}$: ~6 μM), tannic acid ($IC_{50}$: ~20 μM), benserazide ($IC_{50}$: ~20 μM), and NSC67078 ($IC_{50}$: ~0.3 μM) inhibited HCT116 colon cancer cells proliferation with greater potency than AOAA ($IC_{50}$: ~300 μM). In contrast, although a CBS inhibitor in the cell-free assay, aurintricarboxylic acid failed to inhibit HCT116 proliferation at lower concentrations, and stimulated cell proliferation at 300 μM. Copper-containing compounds present in the libraries, were also found to be potent inhibitors of recombinant CBS; however this activity was due to the CBS inhibitory effect of copper ions themselves. However, copper ions, up to 300 μM, did not inhibit HCT116 cell proliferation. Benserazide was only a weak inhibitor of the activity of the other $H_2S$-generating enzymes CSE and 3-MST activity (16% and 35% inhibition at 100 μM, respectively) *in vitro*. Benserazide suppressed HCT116 mitochondrial function and inhibited proliferation of the high CBS-expressing colon cancer cell line HT29, but not the low CBS-expressing line, LoVo. The major benserazide metabolite 2,3,4-trihydroxybenzylhydrazine also inhibited CBS activity and suppressed HCT116 cell proliferation *in vitro*. In an *in vivo* study of nude mice bearing human colon cancer cell xenografts, benserazide (50 mg/kg/day s.q.) prevented tumor growth. *In silico* docking simulations showed that benserazide binds in the active site of the enzyme and reacts with the PLP cofactor by forming reversible but kinetically stable Schiff base-like adducts with the formyl moiety of pyridoxal. We conclude that benserazide inhibits CBS activity and suppresses colon cancer cell proliferation and bioenergetics *in vitro*, and tumor growth *in vivo*. Further pharmacokinetic, pharmacodynamic and preclinical animal studies are necessary to evaluate the potential of repurposing benserazide for the treatment of colorectal cancers.

**Keywords**

Hydrogen sulfide; Cancer; Cell proliferation; Bioenergetics; Nitric oxide

## 1. Introduction

In 1942, as part of his pioneering work that led to the description and characterization of the transsulfuration pathway, Du Vigneaud had noted the production of hydrogen sulfide ($H_2S$) in liver homogenates incubated with homocysteine [1]. We now know that the enzyme responsible for this effect is cystathionine-β-synthase (CBS), a pyridoxal 5'-phosphate (PLP)-dependent enzyme, expressed in various cells of the liver, kidney and the nervous system, where it plays a role in cysteine biosynthesis and degradation [2–6]. CBS is unique among the PLP-dependent enzymes, as it also carries a N-terminal heme prosthetic group coordinated by Cys52 and His65 residues [7,8]. Although heme is not required for

enzymatic activity, its presence can affect its catalytic activity serving as a redox sensor. The C-terminal region of CBS exerts an auto-inhibitory function by partially shielding the active site that can be alleviated by S-adenosyl methionine binding [7,8].

$H_2S$ (a product of CBS-mediated cysteine degradation, as well as several other mammalian enzymes) is well recognized as a signaling molecule in mammals that controls fundamental cellular processes, including growth, differentiation, movement and cell death [3–6]. At a molecular level, $H_2S$ regulates these processes by altering the activity of protein kinases, membrane ion channels and nuclear transcription factors as well key mitochondrial proteins involved in the regulation of cellular bioenergetics [3–6,9,10].

We have recently discovered that CBS is abundantly overexpressed in colon cancers when compared to surrounding normal colonic mucosa; CBS overexpression has also been detected in multiple colon cancer cell lines including HCT116, LoVo and HT29 [11]. The relative overexpression of CBS has also been reported in ovarian, breast and bladder cancers ([12–14], reviewed in [15,16]). Pharmacological inhibition or knockdown of CBS inhibits the proliferation of cancer cell lines and reduces the growth of tumor xenografts *in vivo*, identifying CBS as a preclinically-validated anticancer drug target [11–16]. CBS has also been proposed as a therapeutic target for non-alcoholic fatty liver disease [17] and stroke [18,19].

However, currently there are no potent and selective CBS inhibitors available. Aminooxyacetic acid (AOAA) is commonly referred to as a selective CBS inhibitor, even though it also inhibits another $H_2S$-producing enzyme, cystathionine-gamma lyase (CSE) [20] as well as several transaminases [21–25]. Previous efforts to identify CBS inhibitors from commercially available libraries yielded compounds with relatively low potency and limited CBS selectivity [26,27]. For instance, a recent high-throughput tandem-microwell assay identified 1,6-dimethyl-pyrimido[5,4-e]-1,2,4-triazine-5,7(1H,6H)-dione (NSC67078) as a CBS inhibitor, which, however, also inhibited CSE with a potency that was only 3-fold lower [27]. In a further effort to identify CBS inhibitors, we have conducted a screen of a composite library of 8871 drugs and well-annotated pharmacological compounds. The screen identified several CBS inhibitors including benserazide. Additional studies demonstrated that benserazide is an effective inhibitor of colon cancer cell proliferation *in vitro* and tumor xenograft growth *in vivo*, suggesting its potential for therapeutic repurposing as an antitumor agent.

## 2. Materials and methods

### 2.1. Test compounds

Unless otherwise specified, compounds were obtained from Sigma/Aldrich. Except for the studies using the libraries (which used pre-dissolved drugs in DMSO), all compounds were dissolved freshly prior to each experiment.

### 2.2. Primary screen to identify inhibitors of CBS-derived $H_2S$ production

Recombinant full length human CBS was purchased from Genscript Inc (Piscataway, NJ). The AzMC (7-azido-4-methylcoumarin) based screening (modified from [26]) was carried

out in 96-well plate format on an automated robotic system. This stand-alone robotic system is comprises of a plate washer (EL406, Biotek, Winooski, VT), a dispenser (MicroFlo, Biotek, Winooski, VT), a pipetting station (Precision, Biotek, Winooski, VT), an incubator (Cytomat 2C, Thermo Electron Corporation, Asheville, NC) and plate reader (Synergy 2, Biotek, Winooski, VT) connected with a robotic arm (Twister II, Caliper Life Sciences Inc, Hopkinton, MA). Test compounds, dissolved in dimethyl sulfoxide (DMSO), were added to each well to yield a final concentration of 30 μM (5% DMSO) in a total assay volume of 200 μl. The assay solution contained Tris HCl (50 mM, pH 8.0), human recombinant full-length CBS (5 μg/well), the CBS substrates L-cysteine and homocysteine (each at 2.0 mM final concentration), pyridoxal 5'-phosphate (PLP), (5 μM final concentration), and the $H_2S$-specific fluorescent probe AzMc [26] (10 μM final concentration). The 96 well plates were incubated at 37 °C, and the increase in the AzMc fluorescence in each well was read at 450 nm (λex = 365 nm) over a two-hour time course. A standard curve was generated using different concentrations of the $H_2S$ donor NaHS. The CBS inhibitors AOAA (30 μM) [20] and NSC67078 (30 μM) [27] (1,6-dimethyl-pyrimido[5,4-e]-1,2,4-triazine-5,7(1H,6H)-dione; also known as toxoflavin, xanthothricin and PKF118-310) were used as positive controls. DMSO (5%) was used as a negative control. Data were analyzed in Gen5 and exported to Excel.

### 2.3. Counterscreen to identify compounds that inhibit the fluorescent AzMC signal generated by the $H_2S$ donor GYY4137

The CBS assay outlined above was modified in a way such that instead of recombinant CBS, the $H_2S$ donor GYY4137 [28] (final concentration: 3 mM) was added to the assay mixture to generate the fluorescent AzMC signal. Compounds that inhibited this signal were classified as non-specific inhibitors (either because they scavenge $H_2S$ or because they interfere with the detection method).

### 2.4. Counterscreen to test the inhibitory effect of test compounds using the `methylene blue' assay

The methylene blue assay, commonly used to detect $H_2S$ [20] was modified for 96-well format. Test compounds were added to each well in 10 μl DMSO, to yield a final concentration of 10, 30, or 100 μM. Control wells only received DMSO; positive control wells received the same concentrations of AOAA. The volume of the activity buffer was 50 μl and contained 50 mM Tris HCl (pH 8.0), human recombinant full-length CBS (5 μg/well), the CBS substrates L-cysteine and homocysteine (each at 2.0 mM final concentration), and pyridoxal 5'-phosphate (PLP), (5 μM final concentration). The 96-well plate was sealed with PCR strips and incubated for 2 h at 37 °C. After the incubation, the plate was put directly on ice. Next, the strip was removed from the plate and 60 μl of 1% ZnAc was added followed by 60 μl of 10% TCA. Subsequently, 10 μl of 60 mM *N,N*-dimethyl-*p*-phenylenediamine and 10 μl of 90 mM $FeCl_3$ were added to each well. The plate was incubated for 15 min at room temperature in the dark. The absorbance was read at 650 nm.

### 2.5. Counterscreens to test the effect of benserazide on CSE and 3-MST activity

The AzMC assay, described above, was modified to assess the effect of benserazide on cystathionine-gamma lyase (CSE) and 3-mercaptopyruvate sulfurtransferase (3-MST)

activity. Recombinant human CSE and 3-MST were obtained from Novus Biologicals. For CSE activity, CSE (2 μg per well) was incubated with its substrate, L-cysteine (10 mM) in Tris HCl buffer for 2 h at 37 °C, followed by the detection of $H_2S$ via the AzMC method as described above. For 3-MST activity, 3-MST (2 μg per well) was incubated with its substrate, 3-mercaptopyruvate (10 mM) in Tris HCl buffer for 2 h at 37 °C, followed by the detection of $H_2S$ via the AzMC method as described above.

### 2.6. Cell proliferation assays using the xCELLigence system

To monitor cell proliferation in real time we used the xCELLi-gence system as described [29]. The system measures electrical impedance across interdigitated micro-electrodes integrated on the bottom of tissue culture E-Plates. The impedance measurement provides quantitative information about the biological status of the cells, including cell number, viability and adherence. HCT-116 cells were seeded at a density of 6000 cells/well in 200 μl. 24 h after seeding, cells were treated with different concentrations of aurintricarboxylic acid, benserazide hydrochloride, tannic acid, hexachlorophene or 2,3,4-trihydroxybenzylhydrazine and the proliferation rate of the cells was measured for an additional 48 h. AOAA and NSC67078 were used as positive controls for CBS inhibition.

### 2.7. Assessment of the cytotoxicity of test compounds using the lactate dehydrogenase assay

Lactate dehydrogenase (LDH) release into the culture medium was used for the determination of HCT116 cell death as described [30]. Briefly, 30 μl of supernatant was collected at 48 h and mixed with 100 μl freshly prepared LDH assay reagent containing 85 mM lactic acid, 1 mM nicotinamide adenine dinucleotide ($NAD^+$), 0.27 mM *N*-methylphenazonium methyl sulfate (PMS), 0.528 mM 2-(4-Iodophenyl)-3-(4-nitrophenyl)-5-phenyl-2H-tetrazolium chloride (INT), and 200 mM Tris (pH 8.2). The changes in absorbance were read kinetically at 492 nm for 15 min (kinetic LDH assay) on a monochromator-based reader (Powerwave HT, Biotek) at 37 °C.

### 2.8. Measurement of mitochondrial function using the MTT assay

At 48 h after treatment of HCT116 cells with various test compounds, cells were incubated in medium containing 0.5 mg/ml 3-(4,5-dimethyl-2-thiazolyl)-2,5-diphenyl-2H-tetrazolium bromide (MTT, EMD BioSciences, San Diego, CA) for 1 h at 37 °C at 5% $CO_2$ [DM1] atmosphere as described [30]. The converted formazan dye was dissolved in DMSO and the absorbance was measured at 570 nm on a monochromator-based reader (Powerwave HT, Biotek) at 37 °C.

### 2.9. Extracellular flux analysis and *in vitro* enzyme activity measurements

Extracellular Flux Analysis (XF24 Analyzer, Seahorse Bioscience, Billerica, MA) was used to measure the effect of benserazide (10 μM, 24 h of incubation) on the bioenergetic function of HCT116 cells as described previously [11,31]. The XF24 creates a transient 7-μl chamber in specialized microplates that allows for OCR (oxygen consumption rate) and ECAR (extracellular acidification rate) to be monitored in real time over 2–3 h. The changes of oxygen and proton concentrations are performed in real-time measurements via specific

fluorescent dyes incorporated in Seahorse Flux Pak cartridges. Four key parameters of mitochondrial function (basal respiration, ATP turnover, proton leak, and maximal respiration) were assessed through the sequential use of 1.5 μg/ml oligomycin (ATP synthase inhibitor), 0.5 μM FCCP (oxidative phosphorylation uncoupler), and 2 μM rotenone + 2 μg/ml antimycin A (Complex I and III inhibitors). The difference between the maximal and the basal respirations was considered as the respiratory reserve capacity (the capacity of a cell to generate ATP via oxidative phosphorylation in response to an increased demand for energy). After the injection of oligomycin and the subsequent inhibition of oxidative phosphorylation, ECAR (extracellular acidification rate) was also measured, as an index of the glycolytic capacity of the cells.

### 2.10. *In silico* docking studies

Benserazide was docked as the theoretically predicted PLP adduct in the CBS active site using the Combiglide algorithm (Schrodinger Inc.) as described [32–34]. The algorithm combines accurate ligand-receptor scoring, highly efficient combinatorial docking algorithms and core-hopping technology to design focused libraries and identify new scaffolds. Docking was performed using the IFD induced-fit docking protocol as implemented in Small-Molecule Drug Discovery Suite 2016 (Schrodinger Inc., Small-Molecule Drug Discovery Suite, 2016-1) [32]. The IFD algorithm involves the use of Glide and Prime modules for docking and refinement, respectively, and it enables modeling of structural changes in proteins as an effect of ligand binding. This is achieved by implementing an improved sampling approach where specific sidechain or backbone atoms are allowed to rearrange after iterative cycles of docking and protein refinement [33,34]. In this case, the sidechains of Lys119 and Gln222 were trimmed and Van der Waals atom radii scaling were set to 1 for the protein and 0.8 for the docked ligands. Prior to calculations, the two PLP-benserazide derivatives were prepared in terms of correct protonation states, tautomerism and stereoisomerism using the LigPrep routine (Schrodinger Inc.). The crystal structure of human CBS (pdb id: 1JBQ) was utilized for docking calculations. Protein preparation was performed by the corresponding routine as implemented in Maestro (Schrodinger Inc.). Water molecules of the CBS crystallographic structure were retained according to the ProtPrep default settings.

### 2.11. *In vivo* studies in tumor-bearing mice

All animal studies were approved by the IACUC of UTMB. Athymic male and female mice (8–10 weeks, n = 18) were injected subcutaneously in either the right or left dorsum with $2 \times 10^6$ HT29 cells as described [11]. Three days later, the mice were randomized into two groups and injection subcutaneous (SQ) with either phosphate buffered saline (PBS, n = 9), or benserazide (50 mg/kg/day s.q., n = 9), once per days for the duration of the experiment. Benserazide solutions were made fresh daily, immediately prior to treatment of the animals. Tumor dimensions were measured daily transcutaneously using a caliper. Animal weights were also recorded.

### 2.12. Statistical analysis

Data are presented as mean ± SEM and were analyzed using GraphPad Prism software or SPSS. Statistical analyses included Student-*t* test or one-way ANOVA followed by Bonferroni's multiple comparisons.

## 3. Results

In order to identify novel inhibitors of CBS, we screened 8866 clinically used drugs and well-annotated pharmacological compounds, a composite collection of 11 commercially available libraries and a small custom library assembled from known PLP-dependent enzyme inhibitor compounds consisting of the ornithine decarboxylase inhibitor DL-difluoromethylornithine; the thymidylate synthase, dihydrofolate reductase and glycinamide ribonucleotide formyltransferase inhibitor pemetrexed, the GABA transaminase inhibitor vigabatrin, the GABA transaminase and aromatic L-amino acid decarboxylase inhibitor 3-hydroxybenzylhydrazine and the DOPA decarboxylase inhibitor carbidopa (Table 1). All compounds were screened at a concentration of 30 μM. Compounds that showed >50% CBS inhibition at 30 μM were considered potential hits. The number of potential hits varied between libraries. Some diversity collections (like LOPAC) yielded up to a dozen potential hits, some more specific collections (*e.g.* the ActiTarg P library or the PLP-dependent custom collection) didn't yield any potential hits. When a compound was represented in multiple libraries, it was positively identified as a potential hit compound multiple times, indicating the reliability of the screening assay. Individual CBS activities of all compounds tested (% of vehicle control), organized by libraries, are shown in Fig. 1. The PLP-dependent enzyme inhibitor compounds were also re-tested in a broader concentration-response range (10–100 μM); no inhibitory effects were observed for any of them, except with 3-hydroxybenzylhydrazine, which inhibited CBS activity by 24, 37, and 68%, at 10, 30, and 100 μM, respectively. Carbidopa was a weak inhibitor of CBS activity (6% inhibition at 100 μM).

Confirmatory assays were performed on compounds that were repurchased from commercial sources. The 30 most potent inhibitors of CBS-stimulated AzMC fluorescence signal are shown in Table 2. Taking into account the fact that some of the compounds contain electrophilic moieties, which could directly react with $H_2S$, as well as some of them can quench coumarin fluorescence, potential hit compounds were counterscreened with the $H_2S$ donor GYY4137 in identical reaction conditions. The majority of the potential hit compounds decreased GYY4137-induced AzMC fluorescence (Table 2).

The compounds that could be confirmed as CBS inhibitors with potency comparable to AOAA (and without significantly interfering with GYY4137-induced AzMC fluorescence) are hexachlorophene, tannic acid, aurintricarboxylic acid, and benserazide. These four compounds were further characterized, along with the principal reference compound AOAA [20] and the secondary reference compound, NSC67078 [27]. Inhibitory effect of the two reference compounds and the four identified CBS inhibitors on recombinant CBS and on GYY4137-induced AzMC fluorescence are shown in Table 3; full concentration-response curves shown in Fig. 2. The structures of the six compounds (two reference compounds and four compounds identified by the screen as bona fide CBS inhibitors) are shown in Fig. 3.

The CBS inhibitory effect of hexachlorophene, tannic acid, aurintricarboxylic acid, and benserazide were also confirmed using the methylene blue assay, which detects $H_2S$ production by a different principle than the AzMC assay (Table 3). Unexpectedly, the second reference compound CBS inhibitor NSC67078, in addition to inhibiting CBS-induced AzMC fluorescence with an $IC_{50}$ of ~1 μM, also inhibited GYY6137-induced AzMC fluorescence with an $IC_{50}$ of ~6 μM (Table 3, Fig. 2B) indicating that the observed inhibitory effects are due to a combination of direct CBS inhibition as well as $H_2S$ scavenging and/or interference with the assay used to detect $H_2S$. While conducting confirmatory dose-response work with the four compounds identified as CBS inhibitors, we have noted the aqueous instability of benserazide: while freshly made solutions produced the inhibition depicted above, storage of benserazide stock solutions in aqueous media or DMSO diminished its activity. For instance, while freshly dissolved benserazide at 100 μM inhibited CBS activity by 66 ± 1%, after preparing stock solutions in PBS or DMSO and storing them at −20 °C for 1 week, its potency decreased to 45 ± 4% or 53 ± 3% inhibition of CBS activity, respectively, at 100 μM (n = 3); these data are consistent with prior findings showing the oxidation-prone character of benserazide [35,36].

Hexachlorophene, tannic acid, aurintricarboxylic acid and benserazide, as well as the two reference compounds AOAA (Fig. 4) and NSC67078 (Fig. 5) were next tested on cell proliferation in the HCT116 human colon carcinoma cell line. Cytotoxicity was assessed, in parallel, by the LDH release assay and the MTT assay. AOAA and NSC67078 concentration-dependently inhibited cell proliferation, with $IC_{50}$ values of 300 μM and 0.3 μM, respectively (Figs. 4 and 5). The effect of NSC67078 was also associated with a suppression of MTT conversion (Fig. 5). From the four compounds identified by the CBS screen, hexachlorophene (the least potent CBS inhibitor among the four identified hit compounds), did not affect HCT116 proliferation up to 3 μM, but fully inhibited cell proliferation at 10 μM (Fig. 6). However, at this concentration, the compound also exerted cytotoxic effects, as indicated by the increase in LDH release (Fig. 6C). The polyphenol tannic acid concentration-dependently inhibited proliferation, starting with 10 μM; complete inhibition was seen at 100 μM, without signs of cytotoxicity (Fig. 7). Aurintricarboxylic acid, although it exhibited *in vitro* CBS inhibitory potency comparable to AOAA, did not inhibit cell proliferation at 10–100 μM, while at 300 μM increased cell proliferation (Fig. 8). Although benserazide was less potent at inhibiting recombinant CBS than AOAA in the cell-free assay, it was more potent than AOAA in the proliferation assay. Benserazide inhibited the proliferation of HCT116 cells with a steep dose-response curve. Concentrations up to 10 μM exerted no inhibitory effects, whereas at 30 μM, benserazide completely inhibited HCT116 proliferation. and increased LDH release (Fig. 9).

Among the most potent potential hit compounds identified (Table 2), several of them contained copper, for instance ST012942 and the chlorophyllide $Cu^{2+}$ complex Na salt (contained in the “killer plates” library and the natural product library, respectively). However, ST012861 (a copper-free analogue of ST012942), failed to inhibit recombinant CBS activity (Fig. 10A), suggesting that copper itself may be the inhibitor of CBS activity. In addition to inhibiting CBS-induced AzMC fluorescence, ST012942 also inhibited GYY4137-induced AzMC responses, although with a lower potency ($IC_{50}$: 0.1 μM vs. 1 μM) (Fig. 10B). In a follow-up assay we have tested the effect of three different $Cu^{2+}$ salts

on the activity of recombinant CBS-induced AzMC fluorescence, as well as on GYY4137-induced AzMC fluorescence. As shown in Table 4, all salts: copper(II) chloride; copper(II) acetate and copper(II) nitrate exhibited a potent inhibitory effect on recombinant CBS with an $IC_{50}$ ~ 0.2 μM. A lesser degree of inhibitory effect was also noted on GYY4137- elicited AzMC responses (~15% inhibition at 1 μM; $IC_{50}$, ~1 μM). In fact, the effects of the copper-containing compound ST012942 and the effects of $CuCl_2$ were overlapping, both on CBS- and GYY4137-induced AzMC fluorescence values (Fig. 10). To further investigate the role of CBS inhibition by copper we performed cell proliferation assay in the HCT116 cells. As shown in Fig. 11, copper only inhibited HCT116 cells proliferation at the highest concentration tested (1 mM), which also decreased MTT conversion and LDH activity. The paradoxical reduction in LDH activity is most likely the result of the previously reported [37] direct inhibition of the LDH enzyme by copper ions.

The major benserazide metabolite 2,3,4-trihydroxybenzylhydrazine (THBH, also known as Ro 04-5127) also acted as a CBS inhibitor with potency comparable to benserazide (at 10, 30 and 100 μM, it exerted a 31 ± 2%, 51 ± 2% and 82% inhibition of recombinant CBS activity, n = 3) and inhibited HCT116 cell proliferation *in vitro* at 10–300 μM; it reduced MTT conversion at 300 μM, but did not exert cytotoxic effects, as evidenced by a lack of significant increase of LDH concentrations in the cell culture medium (Fig. 12).

Benserazide contains a free β-hydroxyamine group, which can react with aldehyde groups to produce Schiff bases. To gain insight to the putative mode of CBS inhibition by benserazide, docking calculations were performed by considering the two distinct PLP-benserazide derivatives that could be potentially formed, with either of them potentially representing the actual inhibitor of the protein (Fig. 13). Compound **1** (Fig. 13A, top) is the derivative of the coupling between the free amine of the unmodified benserazide with the formyl functionality of PLP while compound **2** (Fig. 13A, bottom) is the derivative obtained by reaction of the major benserazide metabolite 2,3,4-trihydroxybenzylhydrazine with the respective moiety of PLP. Both molecules are expected to be relatively kinetically stable, as the resulting Schiff bases carry an aromatic ring substitution. Compound **1** and Compound **2** were docked to the PLP-binding site of CBS using an induced-fit docking protocol enabling additional flexibility and enhanced sampling for modeling structural rearrangements of the target upon binding. Docking results showed that although both molecules adopted a highly identical geometry with respect to each other and the crystallographic free PLP cofactor, the PLP-benserazide derivative **1** was systematically bound demonstrating moderately higher docking scores than the corresponding PLP-trihydroxybenzylhydrazine derivative **2** with respective differences of ~1 kcal/mol (best pose score: **1**, −9.91 kcal/mol; **2**, −8.83 kcal/mol). On this basis, the higher affinity predicted for **1** was attributed to the interaction geometry that permitted formation of additional hydrophobic contacts with the protein environment as well as extensive hydrogen bonding interactions between the trihydroxybenzyl ring and polar residues located at the periphery of the cavity such as His203, Tyr223 and Tyr308 with respect to the corresponding, less-favorable interaction geometry of **2** (Fig. 13B,C). While an equilibrium between the two different states of benserazide cannot be ruled out in the assay conditions, docking shows that the two molecules demonstrate a high structural convergence in terms of binding orientation.

The CBS inhibitory potency of benserazide was dependent on the concentration of the substrates used in the assay mixture. Reduction of the concentration of cysteine and homocysteine from 2 mM (our standard assay conditions) to 0.5 mM increased the inhibitory potency of benserazide. For instance, under standard assay conditions, 10 μM benserazide inhibited CBS activity by 29 ± 1%, while under low substrate conditions, the same concentration of benserazide exerted a 61 ± 2% inhibitory effect; n = 3). On the other hand, doubling of substrate concentrations to 10 mM reduced the inhibitory potency of benserazide. For instance, under standard assay conditions, 100 μM benserazide inhibited CBS activity by 66 ± 1%, while under high substrate conditions, the same concentration of benserazide exerted a 10 ± 2% inhibitory effect; n = 3) Benserazide was relatively selective as a CBS inhibitor, because CSE activity was only slightly affected (a 16 ± 6% inhibition at 100 μM; n = 3), while 3-MST activity was unaffected (3-MST activity in the presence of 30, 100 and 300 μM benserazide was 80 ± 14, 60 ± 11 and 50 ± 13% of vehicle control; n = 3).

Benserazide, at 10 μM, exerted an inhibitory effect on the bioenergetics o HCT116 colon cancer cells; it inhibited oxidative phosphorylation/mitochondrial electron transport (Fig. 14A), without significantly affecting glycolysis (Fig. 14B). In addition to HCT116 cells, benserazide also inhibited cell lines proliferation in the colon cancer cell line HT29 (Fig. 15); this cell line – similar to HCT116 cells – expresses high levels of CBS [11]. At 100 μM (but not at lower concentrations) benserazide also exerted cytotoxic effects in HT29 cells (Fig. 15). In contrast, benserazide did not inhibit proliferation in another colon cancer cell line LoVo (Fig. 16); this cell line has a lower expression of CBS, and it expresses high levels of CSE, another $H_2S$-producing enzyme [11]. Finally, benserazide prevented the growth of HT29 subcutaneous xenografts in tumor-bearing nude mice *in vivo* (Fig. 17).

## 4. Discussion

The main conclusions of the current study are the following: (a) from a composite library of 8871 clinically used drugs and well-annotated pharmacological compounds, 4 compounds were identified with CBS inhibitory activity and no non-specific scavenging effects or interference with the assay conditions; these compounds were hexachlorophene, tannic acid, aurintricarboxylic acid and benserazide; (b) three of the identified CBS inhibitors also exerted inhibitory effects on HCT116 cell proliferation, while, unexpectedly, aurintricarboxylic acid failed to inhibit cell proliferation, and, in fact, it exerted stimulatory effects at the highest concentration tested; (c) benserazide was relatively selective as a CBS inhibitor (versus CSE and 3-MST); (d) modeling studies predict that benserazide, in a manner that is similar to the mode of AOAA's action, interacts with the PLP prosthetic group in the active site of CBS, which we view as the likely mode of CBS inhibition; (e) benserazide inhibits colon cancer cell proliferation in the high-CBS-expressor HCT116 and HT29 cell lines, but not in LoVo cells, which express a lower level of CBS; (f) benserazide inhibits cellular bioenergetics in HCT116 cells; and (g) benserazide suppresses colon cancer growth in tumor-bearing mice. Based on these data we suggest that benserazide should be further explored with respect to its potential suitability for therapeutic repurposing for cancer. Additional data presented in the current report confirm previous findings [38,39] demonstrating that copper is a direct inhibitor of CBS activity. Finally, we confirmed that the reference compound AOAA is a CBS inhibitor and antiproliferative agent in colon cancer

cells, while the second reference compound NSC67078 was found to potently inhibit not only the CBS-induced AzMC fluorescence response, but also the $H_2S$ donor GYY4137-induced AzMC fluorescence, suggesting that at least part of the inhibition of the CBS-induced signal is unrelated to direct inhibition of the catalytic activity of CBS. Nevertheless, NSC67078 was found to be a potent inhibitor of HCT116 cell proliferation *in vitro*.

Hexachlorophene (2,2′-methylenebis(3,4,6-trichlorophenol)-3,4,6-trichloro-2-[(2,3,5-trichloro-6-hydroxyphenyl)methyl]phenol) is an organochlorine compound that was once widely used as a disinfectant (a common use being the skin cleansing of newborns), until it was withdrawn due to safety issues [40]. Hexachlorophene is known to have several pharmacological activities, including the inhibition of TAR DNA binding protein [41], inhibition of coronavirus entry [42] and inhibition of amyloid assembly [43]. Hexachlorophene is also known as a glutaminase inhibitor [44] and as an inhibitor of the beta-catenin pathway [45]. It has not been previously identified as a CBS inhibitor or a $H_2S$ biosynthesis inhibitor, even though it has already been shown to inhibit tumor cell proliferation *in vitro*; this effect was attributed to its inhibitory effect on the catenin pathway [46]. Even though hexachlorophene inhibits HCT116 proliferation at fairly low concentrations (10 μM), based on the history and the toxicological profile of the compound we do not believe that therapeutic repurposing of this compound as a CBS inhibitor is a realistic option.

Tannic acid (2,3-dihydroxy-5-({[(2R,3R,4S,5R,6R)-3,4,5,6-tetrakis({3,4-dihydroxy-5-[(3,4,5-trihydroxyphenyl)carbonyloxy]phenyl}carbonyloxy)oxan-2-yl]methoxy}carbonyl)phenyl 3,4,5-trihydroxybenzoate) is a commercial form of tannin, which is a common natural polyphenol product of various plants (Tara pods, gallnuts, Sicilian Sumac leaves). Tannic acid is used in certain food industries, and albumin tannate was used in the 60′s and 70′s as an antidiarrheal agent [47–49]. Thorson and colleagues have previously identified another polyphenol, rutin, as a CBS inhibitor [26]; to our knowledge this is the first report to identify tannic acid as a CBS inhibitor. Although the polyphenolic nature of tannic acid suggested non-specific (*e.g.* potential $H_2S$ scavenging) properties of various polyphenols, tannic acid did not interfere with the AzMc responses induced by the $H_2S$ donor compound GYY4137. Interestingly, tannins have been reported to inhibit bacterial $H_2S$ production [50], an effect that we hypothesize may be related to its inhibitory effect of bacterial $H_2S$-producing enzymes. Tannic acid exerted a concentration-dependent inhibitory effect on HCT116 cell proliferation, with an $IC_{50}$ of 20 μM. Multiple lines of studies have previously identified the anticancer effects of tannins, although the exact mechanism(s) have not been clearly elucidated; they range from direct cytotoxity to inhibition of various putative target enzymes including proteasomes [51–55]. Based on the current studies, we hypothesize that inhibition of tumor CBS activity may contribute to the anticancer effects of tannins.

The next CBS inhibitor identified by our screen was aurintricarboxylic acid, which, to our knowledge, has not been previously identified as a CBS inhibitor. This compound – which has the propensity to polymerization in aqueous solution, forming a stable free radical that has been shown to inhibit various protein-nucleic acid interactions – has previously been shown to possess a number of pharmacological activities, including protease inhibition,

complement inhibition, ribonuclease inhibition and neuraminidase inhibition [56–60]. It has also been shown to stimulate insulin-like growth factor 1 receptor, AKT and ERK signaling [61–63]. The stimulation of cell proliferation by aurintricarboxylic acid observed in our experiments – similar to previously observed stimulation of cell proliferation of various cell lines by this compound [64–66] – may be related to the ability of the compound to stimulate various proliferative signaling pathways; we hypothesize that these actions are more predominant in HCT116 cells that any antiproliferative effects that would be expected via CBS inhibition. Although its mode of action and its diverse pharmacological effects suggest lack of specificity (and perhaps lack of *in vivo* utility) surprisingly, aurintricarboxylic acid is tolerated in experimental animals, and, in fact, has been shown to produce therapeutic benefits in a variety of conditions including encephalitis and sepsis [62,63].

Finally, our screen and our follow-up work identified benserazide (*(RS)*-2-Amino-3-hydroxy-N-(2,3,4-trihydroxybenzyl) propanehydrazide) as a CBS inhibitor with an $IC_{50}$ of ~30 μM. Thorson and colleagues have previously reported [26] the CBS inhibitory effect of benserazide, albeit with a lower potency (125 μM). We hypothesize that the difference may be related to the aqueous instability (oxidation-prone nature) of this compound – as demonstrated in our current study as well as reported previously [35,36]. Benserazide produced the expected features of a CBS inhibitor; similar to AOAA (as shown previously in [11,67]), benserazide inhibited colon cancer cell proliferation, and suppressed cancer cell bioenergetic responses. Our computer-based modeling studies have identified a predicted mode of its inhibitory action. It should be noted, nevertheless, that the extent to which benserazide suppresses the proliferation of colon cancer cells depended on the cell type studied. A significant suppression of proliferation (and, at the highest concentrations tested, some degree of cytotoxicity, as evidenced by increased LDH release) was noted in HCT116 cells (Fig. 9) and HT-29 cells (Fig. 15) that express a relatively high concentration of CBS. By comparison, in LoVo cells, which express a lower level of CBS, neither benserazide-induced antiproliferative effects, nor benserazide-induced increases in LDH release were seen (Fig. 16). These data support the conclusion that benserazide is targeting CBS. However, we are well aware of the fact that there are many other possibilities that may explain the differential effects, including potential differences in cell uptake, or potential differences in the cellular metabolism of benserazide.

Benserazide is one component of a two-component oral anti-Parkinson therapeutic combination (with the other component being L-DOPA) [68,69]. The original mode of benserazide's mode of action is to inhibit the peripheral DOPA decarboxylase (which, similar to CBS, is a PLP-dependent enzyme) [68,69]. A detailed review of the published pharmacological and toxicological literature from the 70′s [70,71] – mainly generated by pharmacologists at Hoffman LaRoche, the original producer of Madopar® Roche (1 component benserazide + 4 component L-DOPA) – reveals that benserazide has >35% oral bioavailability in rats and ~70% oral bioavailability in humans. At 1–4 h after oral administration of a single dose of 50 mg radiolabeled benserazide, human plasma concentrations were established in the range of 0.5–1 μg/ml (*i.e.* 2–4 μM). In rats, a single dose of 10 mg radiolabeled benserazide produced plasma levels of 1–10 μg/ml (*i.e.* 4–40 μM) [70,71]. Similar to many examples in the literature, the plasma concentrations of drugs targeting intracellular enzymes (especially when the mode of action is irreversible binding to

the enzyme, as is the case for benserazide, which binds to the PLP prosthetic group of its targets) do not necessarily predict tissue levels or the degree of inhibition of its intracellular target. Importantly, in rat studies [70,71], benserazide concentrations in the kidney and the liver were 2–3-fold higher than plasma concentrations at 1–12 h after single dose administration. In addition to benserazide itself, our data indicate that its major metabolite 2,3,4-trihydroxybenzylhydrazine (THBH) also acts as a CBS inhibitor and colon cancer cell antiproliferative agent (Fig. 12). Based on the above pharmacokinetic considerations, we predict that tumor tissue concentrations comparable to the antiproliferative concentrations of benserazide (as well as its metabolite) may be achievable *in vivo*, which may open the potential for therapeutic repurposing of the compound.

One way to predict target engagement is to survey the literature for biochemical alterations (potential biomarkers) after benserazide administration that may suggest CBS inhibition. We found no published studies in the literature on the effect of benserazide on $H_2S$ production or $H_2S$ levels. Therefore, we focused on secondary biomarkers. Since liver CBS plays a physiological role in plasma homocysteine metabolism [15], we predicted that CBS target engagement by benserazide in humans may induce hyperhomocysteinemia. Indeed, a recent study shows that benserazide in Parkinson's patients produces a ~15% increase in plasma homocysteine levels [72], which we interpret as the inactivation of CBS by benserazide, followed by the accumulation of its substrate, homocysteine in the circulation. Further pharmacokinetic and pharmacodynamic studies are needed to determine the feasibility of benserazide as a potentially repurposable agent for the experimental therapy of cancer.

One side-finding of the current work was the “re–rediscovery” of the inhibitory effect of copper ions on CBS activity; a finding that has already been described in 1958 by Matsuo and Greenberg [36], and re-discovered by the Kraus group in 2005 [37]. Although the potency of copper was found to be remarkable – in fact, copper is technically the most potent CBS inhibitor “compound” known to date – free copper ions did not exert antiproliferative effects in HCT116 cells, probably due to limited cell uptake, as well as the high ability of cells to sequester and neutralize any free copper ions [73,74]. Future work is needed to determine whether the ability of copper to inhibit CBS may be useful in the context of therapeutic CBS inhibition.

Another side finding of the current project was the discovery that the second reference CBS inhibitor compound, NSC67078 [27] potently inhibits not only the CBS-induced AzMC fluorescence response, but also the $H_2S$ donor GYY4137-induced AzMC fluorescence, suggesting that at least part of the inhibition of the CBS-induced signal is unrelated to direct inhibition of the catalytic activity of CBS. Nevertheless, NSC67078 was found to be the most potent inhibitor of HCT116 cell proliferation amongst all the molecules evaluated in the current project. Given the fact, however, that this compound is known as a highly potent inhibitor of the β-catenin pathway [75,76], as well as a SIRT1/2 inhibitor [77], we hypothesize that β-catenin inhibition and SIRT inhibition significantly contributes to its potent inhibitory effect on cancer cell proliferation *in vitro*; further work is needed to dissect the various possible mechanisms (β-catenin inhibition, SIRT inhibition, CBS inhibition, perhaps other actions as well) in its anti-proliferative actions.

A third side-finding of the current studies demonstrates that none of the known PLP-dependent enzyme inhibitors exerted potent inhibitory effects on CBS. Prior studies have demonstrated that PAG (a PLP-dependent inhibitor of CSE) is not an inhibitor of CBS [20]. Similarly, D-cycloserine and isoniazid, two antibiotics that suppress M. tuberculosis infection via inhibition of multiple PLP-dependent enzymes, failed to act as significant inhibitors of CBS activity (15–20% inhibition at 1 mM) [20]. Based on these data, we conclude that PLP-dependent enzyme inhibition is not a sufficient criterion for CBS inhibition.

Taken together, the current work characterized the potency, selectivity and the antiproliferative and bioenergetic actions of benserazide, one of the CBS inhibitors identified through *in vitro* screening. Based on the findings reported in the current article, we conclude that benserazide may be potentially suitable for repurposing for the treatment of colorectal cancers, although further pharmacokinetic, pharmacodynamic and preclinical animal studies are necessary.

## Acknowledgements

Part of this work was supported by the National Institutes of Health (R41CA18628801 and R01CA17580303) and the Cancer Prevention Research Institute of Texas (DP150074).

## Abbreviations

| | |
|---|---|
| **AOAA** | aminooxyacetic acid |
| **AzMC** | 7-azido-4-methylcoumarin |
| **CBS** | cystathionine-beta-synthase |
| **CSE** | cystathionine-gamma lyase |
| **DMSO** | dimethylsulfoxide |
| **$H_2S$** | hydrogen sulfide |
| **3-MST** | 3-mercaptopyruvate sulfurtransferase |
| **PLP** | pyridoxal 5' phosphate |
| **THBH** | 2,3,4-trihydroxybenzylhydrazine. |

## References

[1]. Binkley F, du Vigneaud V. The formation of cysteine from homocysteine and serine by liver tissue of rats. J. Biol. Chem. 1942; 144:507–511.

[2]. Miles EW, Kraus JP. Cystathionine beta-synthase: structure, function, regulation, and location of homocystinuria-causing mutations. J. Biol. Chem. Jul; 2004 279(29):29871–29874. [PubMed: 15087459]

[3]. Kamoun P. Endogenous production of hydrogen sulfide in mammals. Amino Acids. Jun; 2004 26(3):243–254. [PubMed: 15221504]

[4]. Jhee KH, Kruger WD. The role of cystathionine beta-synthase in homocysteine metabolism. Antioxid. Redox Signal. May-Jun;2005 7(5–6):813–822. [PubMed: 15890029]

[5]. Fiorucci S, Distrutti E, Cirino G, Wallace JL. The emerging roles of hydrogen sulfide in the gastrointestinal tract and liver. Gastroenterology. Jul; 2006 131(1):259–271. [PubMed: 16831608]

[6]. Wang R. Physiological implications of hydrogen sulfide: a whiff exploration that blossomed. Physiol. Rev. Apr; 2012 92(2):791–896. [PubMed: 22535897]

[7]. Ereño-Orbea J, Majtan T, Oyenarte I, Kraus JP, Martínez-Cruz LA. Structural insight into the molecular mechanism of allosteric activation of human cystathionine β-synthase by S-adenosylmethionine. Proc. Natl. Acad. Sci. U. S. A. Sep; 2014 111(37):E3845–E3852. [PubMed: 25197074]

[8]. Majtan T, Pey AL, Fernández R, Fernández JA, Martínez-Cruz LA, Kraus JP. Domain organization, catalysis and regulation of eukaryotic cystathionine beta-synthases. PLoS One. Aug.2014 9(8):e105290. [PubMed: 25122507]

[9]. Szabo C. Hydrogen sulphide and its therapeutic potential. Nat. Rev. Drug Discov. Nov; 2007 6(11):917–935. [PubMed: 17948022]

[10]. Li L, Rose P, Moore PK. Hydrogen sulfide and cell signaling. Annu. Rev. Pharmacol. Toxicol. 2011; 51:169–187. [PubMed: 21210746]

[11]. Szabo C, Coletta C, Chao C, Módis K, Szczesny B, Papapetropoulos A, Hellmich MR. Tumor-derived hydrogen sulfide, produced by cystathionine-β-synthase, stimulates bioenergetics, cell proliferation, and angiogenesis in colon cancer. Proc. Natl. Acad. Sci. U. S. A. Jul; 2013 110(30): 12474–12479. [PubMed: 23836652]

[12]. Bhattacharyya S, Saha S, Giri K, Lanza IR, Nair KS, Jennings NB, Rodriguez-Aguayo C, Lopez-Berestein G, Basal E, Weaver AL, Visscher DW, Cliby W, Sood AK, Bhattacharya R, Mukherjee P. Cystathionine beta-synthase (CBS) contributes to advanced ovarian cancer progression and drug resistance. PLoS One. Nov.2013 8(11):e79167. [PubMed: 24236104]

[13]. Sen S, Kawahara B, Gupta D, Tsai R, Khachatryan M, Roy-Chowdhuri S, Bose S, Yoon A, Faull K, Farias-Eisner R, Chaudhuri G. Role of cystathionine β-synthase in human breast cancer. Free Radic. Biol. Med. Sep.2015 86:228–238. [PubMed: 26051168]

[14]. Gai JW, Qin W, Liu M, Wang HF, Zhang M, Li M, Zhou WH, Ma QT, Liu GM, Song WH, Jin J, Ma HS. Expression profile of hydrogen sulfide and its synthases correlates with tumor stage and grade in urothelial cell carcinoma of bladder. Urol. Oncol. Apr; 2016 34(4):166. e15–e20.

[15]. Hellmich MR, Coletta C, Chao C, Szabo C. The therapeutic potential of cystathionine β-synthetase/hydrogen sulfide inhibition in cancer. Antioxid. Redox Signal. Feb; 2015 22(10):424–448. [PubMed: 24730679]

[16]. Szabo C. Gasotransmitters in cancer: from pathophysiology to experimental therapy. Nat. Rev. Drug Discov. Mar; 2016 15(3):185–203. [PubMed: 26678620]

[17]. Sarna LK, Siow YL, K O. The CBS/CSE system: a potential therapeutic target in NAFLD? Can. J. Physiol. Pharmacol. Janruary;2015 93(1):1–11. [PubMed: 25493326]

[18]. Chan SJ, Chai C, Lim TW, Yamamoto M, Lo EH, Lai MK, Wong PT. Cystathionine β-synthase inhibition is a potential therapeutic approach to treatment of ischemic injury. ASN Neuro. Apr. 2015 7(2) 1759091415578711.

[19]. McCune CD, Chan SJ, Beio ML, Shen W, Chung WJ, Szczesniak LM, Chai C, Koh SQ, Wong PT, Berkowitz DB. Zipped synthesis by cross-metathesis provides a cystathionine β-synthase inhibitor that attenuates cellular $H_2S$ levels and reduces neuronal infarction in a rat ischemic stroke model. ACS Cent Sci. Apr; 2016 2(4):242–252. [PubMed: 27163055]

[20]. Asimakopoulou A, Panopoulos P, Chasapis CT, Coletta C, Zhou Z, Cirino G, Giannis A, Szabo C, Spyroulias GA, Papapetropoulos A. Selectivity of commonly used pharmacological inhibitors for cystathionine β synthase (CBS) and cystathionine γ lyase (CSE). Br. J. Pharmacol. Jun; 2013 169(4):922–932. [PubMed: 23488457]

[21]. Cornell NW, Zuurendonk PF, Kerich MJ, Straight CB. Selective inhibition of alanine aminotransferase and aspartate aminotransferase in rat hepatocytes. Biochem. J. Jun; 1984 220(3):707–716. [PubMed: 6466297]

[22]. Sherry AD, Zhao P, Wiethoff AJ, Jeffrey FM, Malloy CR. Effects of aminooxyacetate on glutamate compartmentation and TCA cycle kinetics in rat hearts. Am. J. Physiol. Feb; 1998 274(2 Pt 2):H591–H599. [PubMed: 9486263]

[23]. Kurozumi Y, Abe T, Yao WB, Ubuka T. Experimental beta-alaninuria induced by (aminooxy)acetate. Acta Med. Okayama. Feb; 1999 53(1):13–18. [PubMed: 10096733]

[24]. Dever JT, Elfarra AA. L-methionine-dl-sulfoxide metabolism and toxicity in freshly isolated mouse hepatocytes: gender differences and inhibition with aminooxyacetic acid. Drug Metab. Dispos. Nov; 2008 36(11):2252–2260. [PubMed: 18687801]

[25]. Walczak K, Dąbrowski W, Langner E, Zgrajka W, Piłat J, Kocki T, Rzeski W, Turski WA. Kynurenic acid synthesis and kynurenine aminotransferases expression in colon derived normal and cancer cells. Scand. J. Gastroenterol. Jul; 2011 46(7–8):903–912. [PubMed: 21615226]

[26]. Thorson MK, Majtan T, Kraus JP, Barrios AM. Identification of cystathionine β-synthase inhibitors using a hydrogen sulfide selective probe. Angew. Chem. Int. Ed. Engl. Apr; 2013 52(17):4641–4644. [PubMed: 23512751]

[27]. Zhou Y, Yu J, Lei X, Wu J, Niu Q, Zhang Y, Liu H, Christen P, Gehring H, Wu F. High-throughput tandem-microwell assay identifies inhibitors of the hydrogen sulfide signaling pathway. Chem. Commun. (Camb.). Dec; 2013 49(100):11782–11784. [PubMed: 24213681]

[28]. Li L, Whiteman M, Guan YY, Neo KL, Cheng Y, Lee SW, Zhao Y, Baskar R, Tan CH, Moore PK. Characterization of a novel, water-soluble hydrogen sulfide-releasing molecule (GYY4137): new insights into the biology of hydrogen sulfide. Circulation. May; 2008 117(18):2351–2360. [PubMed: 18443240]

[29]. Ozsvári B, Puskás LG, Nagy LI, Kanizsai I, Gyuris M, Madácsi R, Fehér LZ, Gerö D, Szabo C. A cell-microelectronic sensing technique for the screening of cytoprotective compounds. Int. J. Mol. Med. Apr; 2010 25(4):525–530. [PubMed: 20198300]

[30]. Gerö D, Szabo C. Glucocorticoids suppress mitochondrial oxidant production via upregulation of uncoupling protein 2 in hyperglycemic endothelial cells. PLoS One. Apr.2016 11(4):e0154813. [PubMed: 27128320]

[31]. Coletta C, Módis K, Szczesny B, Brunyánszki A, Oláh G, Rios EC, Yanagi K, Ahmad A, Papapetropoulos A, Szabo C. Regulation of vascular tone, angiogenesis and cellular bioenergetics by the 3-mercaptopyruvate sulfurtransferase/$H_2S$ pathway: functional impairment by hyperglycemia and restoration by DL-α-lipoic acid. Mol. Med. Feb; 2015 21(4):1–14. [PubMed: 25715337]

[32]. Small-Molecule Drug Discovery Suite 2016-1: Schrödinger Suite 2016-1 Induced Fit Docking protocol. Glide version 7.0. Schrödinger, LLC; New York, NY: 2016. Prime version 4.3, Schrödinger, LLC, New York, NY, 2016

[33]. Farid R, Day T, Friesner RA, Pearlstein RA. New insights about HERG blockade obtained from protein modeling, potential energy mapping, and docking studies. Bioorg. Med. Chem. 2006; 14:3160–3173. [PubMed: 16413785]

[34]. Sherman W, Beard HS, Farid R. Use of an induced fit receptor structure in virtual screening. Chem. Biol. Drug Des. 2006; 67:83–84. [PubMed: 16492153]

[35]. Holzgrabe U, Diehl BWK, Wawer I. NMR spectroscopy in pharmacy. J. Pharm. Biomed. Anal. 1998; 17:557–616. [PubMed: 9682143]

[36]. Gasser UE, Fischer A, Timmermans JP, Arnet I. Pharmaceutical quality of seven generic Levodopa/Benserazide products compared with original Madopar®/Prolopa®. Pharmacol. Toxicol. Apr.2013 14:24.

[37]. Dobryszycka W, Owczarek H. Effects of lead, copper, and zinc on the rat's lactate dehydrogenase in vivo and in vitro. Arch. Toxicol. Aug; 1981 48(1):21–27. [PubMed: 7283746]

[38]. Matsuo Y, Greenberg DM. A crystalline enzyme that cleaves homoserine and cystathionine. II. Prosthetic group. J. Biol. Chem. Feb; 1958 230(2):561–571. [PubMed: 13525372]

[39]. Bar-Or D, Rael LT, Thomas GW, Kraus JP. Inhibitory effect of copper on cystathionine beta-synthase activity: protective effect of an analog of the human albumin N-terminus. Protein Pept. Lett. Apr; 2005 12(3):271–273. [PubMed: 15777277]

[40]. Kimbrough RD. Review of the toxicity of hexachlorophene, including its neurotoxicity. J. Clin. Pharmacol. Nov-Dec;1973 13(11):439–444. [PubMed: 4206035]

[41]. Narayan M, Peralta DA, Gibson C, Zitnyar A, Jinwal UK. An optimized InCell Western screening technique identifies hexachlorophene as a novel potent TDP43 targeting drug. J. Biotechnol. Aug.2015 207:34–38. [PubMed: 25987361]

[42]. Cao J, Forrest JC, Zhang X. A screen of the NIH Clinical Collection small molecule library identifies potential anti-coronavirus drugs. Antivir. Res. Feb.2015 114:1–10. [PubMed: 25451075]

[43]. Kirschner DA, Gross AA, Hidalgo MM, Inouye H, Gleason KA, Abdelsayed GA, Castillo GM, Snow AD, Pozo-Ramajo A, Petty SA, Decatur SM. Fiber diffraction as a screen for amyloid inhibitors. Curr. Alzheimer Res. Jun; 2008 5(3):288–307. [PubMed: 18537544]

[44]. Polletta L, Vernucci E, Carnevale I, Arcangeli T, Rotili D, Palmerio S, Steegborn C, Nowak T, Schutkowski M, Pellegrini L, Sansone L, Villanova L, Runci A, Pucci B, Morgante E, Fini M, Mai A, Russo MA, Tafani M. SIRT5 regulation of ammonia-induced autophagy and mitophagy. Autophagy. 2015; 11(2):253–270. [PubMed: 25700560]

[45]. Park S, Gwak J, Cho M, Song T, Won J, Kim DE, Shin JG, Oh S. Hexachlorophene inhibits Wnt/beta-catenin pathway by promoting Siah-mediated beta-catenin degradation. Mol. Pharmacol. Sep; 2006 70(3):960–966. [PubMed: 16735606]

[46]. Cho IR, Koh SS, Min HJ, Kim SJ, Lee Y, Park EH, Ratakorn S, Jhun BH, Oh S, Johnston RN, Chung YH. Pancreatic adenocarcinoma up-regulated factor (PAUF) enhances the expression of β-catenin, leading to a rapid proliferation of pancreatic cells. Exp. Mol. Med. Feb; 2011 43(2): 82–90. [PubMed: 21196815]

[47]. Tannic acid and tannins, IARC Monogr. Eval. Carcinog. Risk Chem. Man. 1976; 10:253–262. [PubMed: 186387]

[48]. Morton JF. Widespread tannin intake via stimulants and masticatories, especially guarana, kola nut, betel vine, and accessories. Basic Life Sci. 1992; 59:739–765. [PubMed: 1417698]

[49]. Gámiz Gracia L, Luque de Castro MD. Development and validation of a flow-injection method for the determination of albumin tannate, the active component of a pharmaceutical preparation. J. Pharm. Biomed. Anal. Janruary;1997 15(4):447–452. [PubMed: 8953487]

[50]. Whitehead TR, Spence C, Cotta MA. Inhibition of hydrogen sulfide, methane, and total gas production and sulfate-reducing bacteria in vitro swine manure by tannins, with focus on condensed quebracho tannins. Appl. Microbiol. Biotechnol. Sep; 2013 97(18):8403–8409. [PubMed: 23149758]

[51]. Kashiwada Y, Nonaka G, Nishioka I, Chang JJ, Lee KH. Antitumor agents, 129. Tannins and related compounds as selective cytotoxic agents. J. Nat. Prod. 1992; 55(8):1033–1043. [PubMed: 1431932]

[52]. Shen M, Chan TH, Dou QP. Targeting tumor ubiquitin-proteasome pathway with polyphenols for chemosensitization. Anticancer Agents Med. Chem. Oct; 2012 12(8):891–901. [PubMed: 22292765]

[53]. Harlev E, Nevo E, Lansky EP, Lansky S, Bishayee A. Anticancer attributes of desert plants: a review. Anticancer Drugs. Mar; 2012 23(3):255–271. [PubMed: 22217921]

[54]. Booth BW, Inskeep BD, Shah H, Park JP, Hay EJ, Burg KJ. Tannic acid preferentially targets estrogen receptor-positive breast cancer. Int. J. Breast Cancer. 2013; 2013:369609. [PubMed: 24369505]

[55]. Zhao HJ, Liu T, Mao X, Han SX, Liang RX, Hui LQ, Cao CY, You Y, Zhang LZ. Fructus phyllanthi tannin fraction induces apoptosis and inhibits migration and invasion of human lung squamous carcinoma cells in vitro via MAPK/MMP pathways. Acta Pharmacol. Sin. Jun; 2015 36(6):758–768. [PubMed: 25864648]

[56]. Blumenthal T, Landers TA. The inhibition of nucleic- acid binding proteins by aurintricarboxylic acid. Biochem. Biophys. Res. Commun. 1973; 55:680–688. [PubMed: 4586617]

[57]. Skidmore AF, Beebee TJ. Characterization and use of the potent ribonuclease inhibitor aurintricarboxylic acid for the isolation of RNA from animal tissues. Biochem. J. 1989; 263(1): 73–80. [PubMed: 2481441]

[58]. Hashem AM, Flaman AS, Farnsworth A, Brown EG, van Domselaar G, He R, Li X. Aurintricarboxylic acid is a potent inhibitor of influenza A and B virus neuraminidases. PLoS One. 2009; 4(12):e8350. [PubMed: 20020057]

[59]. Lipo E, Cashman SM, Kumar-Singh R. Aurintricarboxylic acid inhibits complement activation, membrane attack complex, and choroidal neovascularization in a model of macular degeneration. Invest. Ophthalmol. Vis. Sci. Oct; 2013 54(10):7107–7114. [PubMed: 24106121]

[60]. Lee M, Narayanan S, McGeer EG, McGeer PL. Aurin tricarboxylic acid protects against red blood cell hemolysis in patients with paroxysmal nocturnal hemoglobinemia. PLoS One. Janruary;2014 9(1):e87316. [PubMed: 24489894]

[61]. Pattingre S, Bauvy C, Codogno P. Amino acids interfere with the ERK1/2-dependent control of macroautophagy by controlling the activation of Raf-1 in human colon cancer HT-29 cells. J. Biol. Chem. May; 2003 278(19):16667–16674. [PubMed: 12609989]

[62]. Zhang F, Wei W, Chai H, Xie X. Aurintricarboxylic acid ameliorates experimental autoimmune encephalomyelitis by blocking chemokine-mediated pathogenic cell migration and infiltration. J. Immunol. Feb; 2013 190(3):1017–1025. [PubMed: 23267022]

[63]. Laufenberg LJ, Kazi AA, Lang CH. Salutary effect of aurintricarboxylic acid on endotoxin- and sepsis-induced changes in muscle protein synthesis and inflammation. Shock. May; 2014 41(5): 420–428. [PubMed: 24430547]

[64]. Andrew DJ, Hay AW, Evans SW. Aurintricarboxylic acid inhibits apoptosis and supports proliferation in a haemopoietic growth-factor dependent myeloid cell line. Immunopharmacology. Janruary;1999 41(1):1–10. [PubMed: 9950264]

[65]. Liu C, Chu I, Hwang S. Aurintricarboxylic acid exerts insulin-like growth stimulating effects on Chinese hamster ovary cells under serum-free conditions. J. Biosci. Bioeng. 2001; 91(6):576–580. [PubMed: 16233042]

[66]. Lee TY, Chen WS, Huang YA, Liu TW, Hwang E, Tseng CP. Application of aurintricarboxylic acid for the adherence of mouse P19 neurons and primary hippocampal neurons to noncoated surface in serum-free culture. Biotechnol. Prog. Nov-Dec;2012 28(6):1566–1574. [PubMed: 23011767]

[67]. Chao C, Zatarain JR, Ding Y, Coletta C, Mrazek AA, Druzhyna N, Johnson P, Chen H, Hellmich JL, Asimakopoulou A, Yanagi Y, Olah G, Szoleczky P, Törö G, Bohanon FJ, Cheema M, Lewis L, Eckelbarger D, Ahmad A, Módis K, Untereiner A, Szczesny B, Papapetropoulos A, Zhou J, Hellmich MR, Szabo C. Cystathionine-beta-synthase inhibition for colon cancer: enhancement of the efficacy of aminooxyacetic acid via the prodrug approach. Mol. Med. 2016 in press.

[68]. Rinne UK, Mölsä P. Levodopa with benserazide or carbidopa in Parkinson disease. Neurology. Dec; 1979 29(12):1584–1589. [PubMed: 574221]

[69]. Amadasi A, Bertoldi M, Contestabile R, Bettati S, Cellini B, di Salvo ML, Borri-Voltattorni C, Bossa F, Mozzarelli A. Pyridoxal 5'-phosphate enzymes as targets for therapeutic agents. Curr. Med. Chem. 2007; 14(12):1291–1324. [PubMed: 17504214]

[70]. Schwartz DE, Jordan JC, Ziegler WH. Pharmacokinetics of the decarboxylase inhibitor benserazide in man; its tissue distribution in the rat. Eur. J. Clin. Pharmacol. 1974; 7:39–45. [PubMed: 4853605]

[71]. Schwartz DE, Brandt R. Pharmacokinetic and metabolic studies of the decarboxylase inhibitor benserazide in animals and man. Arzneimittelforschung. 1978; 28:302–307. [PubMed: 580398]

[72]. Müller T, Kuhn W. Homocysteine levels after acute levodopa intake in patients with Parkinson's disease. Mov. Disord. 2009; 24:1339–1343. [PubMed: 19425084]

[73]. Gaetke LM, Chow CK. Copper toxicity, oxidative stress, and antioxidant nutrients. Toxicology. Jul; 2003 189(1–2):147–163. [PubMed: 12821289]

[74]. Ogra Y. Molecular mechanisms underlying copper homeostasis in mammalian cells. Nihon Eiseigaku Zasshi. 2014; 69(2):136–145. [PubMed: 24858509]

[75]. Leow PC, Tian Q, Ong ZY, Yang Z, Ee PL. Antitumor activity of natural compounds, curcumin and PKF118-310, as Wnt/β-catenin antagonists against human osteosarcoma cells. Invest. New Drugs. Dec; 2010 28(6):766–782. [PubMed: 19730790]

[76]. Antony L, van der Schoor F, Dalrymple SL, Isaacs JT. Androgen receptor (AR) suppresses normal human prostate epithelial cell proliferation via AR/β-catenin/TCF-4 complex inhibition of c-MYC transcription. Prostate. Aug; 2014 74(11):1118–1131. [PubMed: 24913829]

[77]. Choi G, Lee J, Ji JY, Woo J, Kang NS, Cho SY, Kim HR, Ha JD, Han SY. Discovery of a potent small molecule SIRT1/2 inhibitor with anticancer effects. Int. J. Oncol. Oct; 2013 43(4):1205–1211. [PubMed: 23900402]

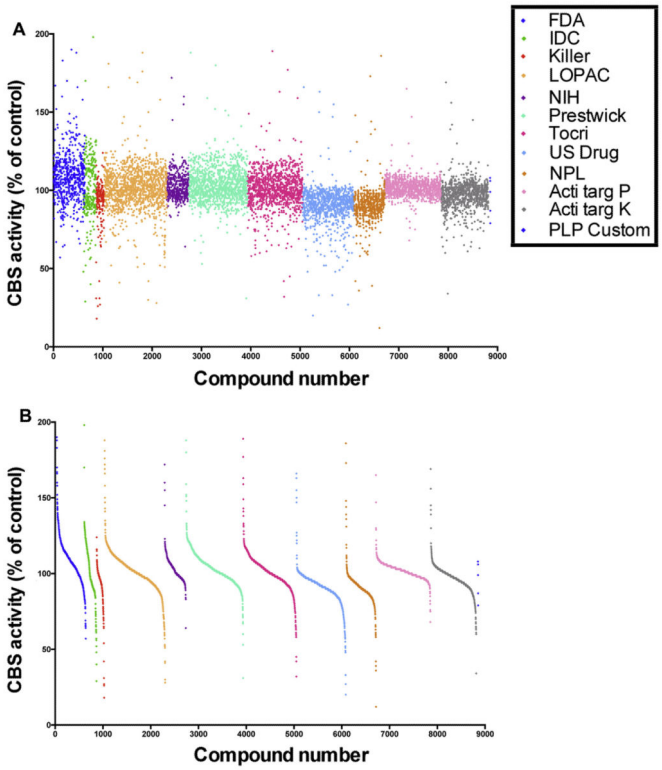


**Fig. 1.**

Scatterplots of the data obtained by the screening of the against CBS. Screening was conducted at a single concentration (30 μM) in 96-plate format using a robotic system. The various libraries are illustrated by different colors; each dot represents an individual compound tested. Part (A) shows the compounds in the order they were tested and (B) shows them after rank-ordering, by individual library, based on their effect on CBS-induced AzMC fluorescence.

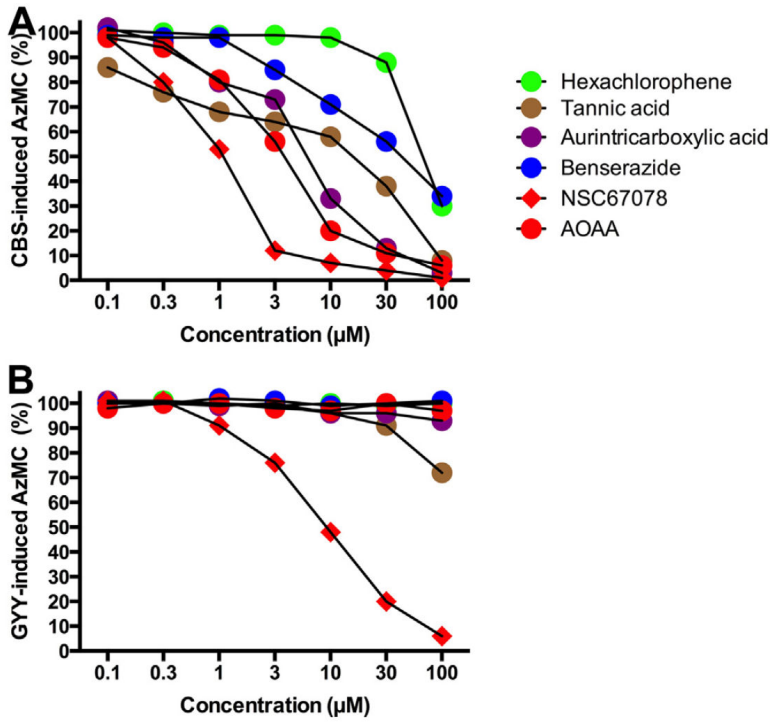


**Fig. 2.**

Effect of hexachlorophene, tannic acid, aurintricarboxylic acid and benserazide and the two reference compounds AOAA and NSC67078 (0.1–100 μM) on (A) CBS-induced AzMC fluorescence and (B) GYY4187-induced AzMC fluorescence. Data represent mean values of triplicate determinations; SEM values are contained within the symbols.

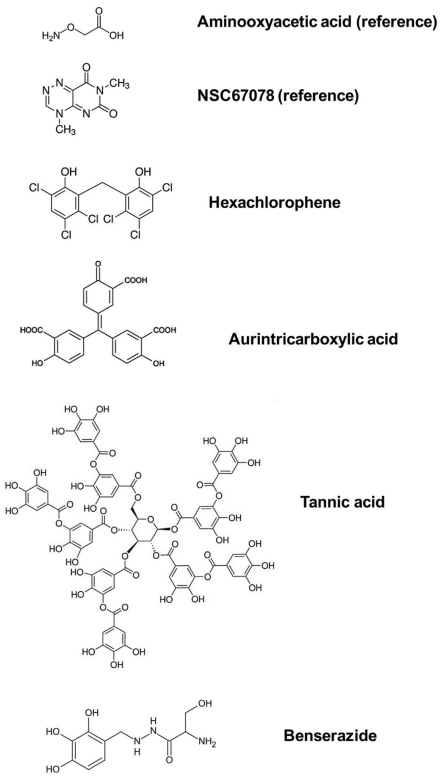


**Fig. 3.**

Structures of the two reference compounds (AOAA and NSC67078) and the four compounds identified by the screen as bona fide CBS inhibitors (hexachlorophene, tannic acid, aurintricarboxylic acid and benserazide).

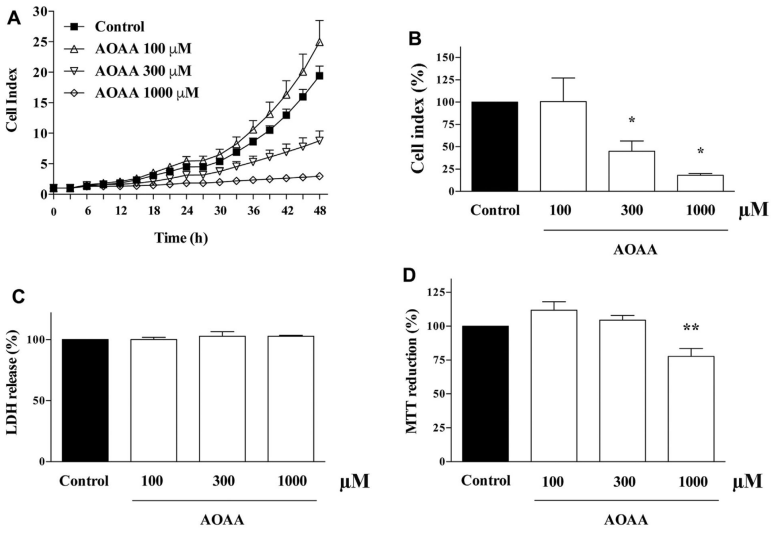


**Fig. 4.**

Effect of the reference compound AOAA (100 μM, 300 μM, 1 mM) on HCT116 cell proliferation and viability. (A): time-course of Cell Index, shown in a representative experiment; (B): summary data of Cell Index at 48 h; vehicle control values are normalized as 100%; (C): LDH release data at 48 h; vehicle control values are normalized as 100%; (D): MTT conversion data; vehicle control values are normalized as 100%. Data shown represent mean ± SEM of n = 5 experiments; *p < 0.05 and **p < 0.01 show significant differences compared to vehicle control.

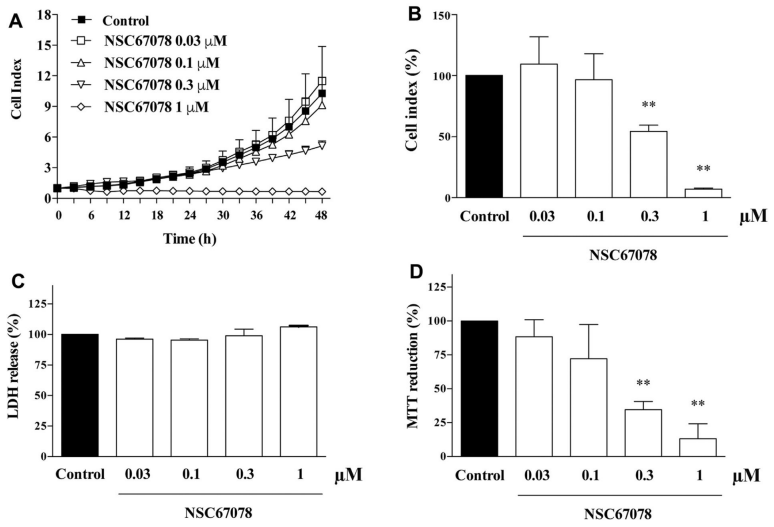


**Fig. 5.**

Effect of the reference compound NSC67078 (30 nM, 100 nM, 300 nM, 1 μM) on HCT116 cell proliferation and viability. (A): time-course of Cell Index, shown in a representative experiment; (B): summary data of Cell Index at 48 h; vehicle control values are normalized as 100%; (C): LDH release data at 48 h; vehicle control values are normalized as 100%; (D): MTT conversion data; vehicle control values are normalized as 100%. Data shown represent mean ± SEM of n = 5 experiments; **p < 0.01 shows significant differences compared to vehicle control.

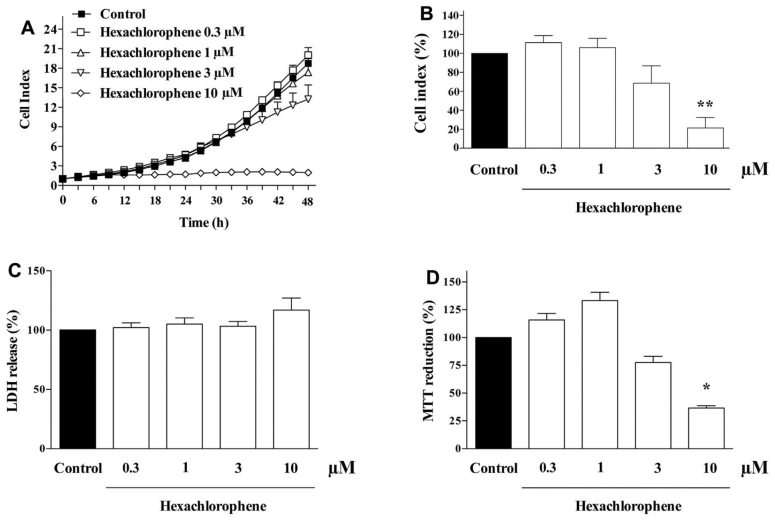


**Fig. 6.**

Effect of hexachlorophene (300 nM, 1 µM, 3 µM, 10 µM) on HCT116 cell proliferation and viability. (A): time-course of Cell Index, shown in a representative experiment; (B): summary data of Cell Index at 48 h; vehicle control values are normalized as 100%; (C): LDH release data at 48 h; vehicle control values are normalized as 100%; (D): MTT conversion data; vehicle control values are normalized as 100%. Data shown represent mean ± SEM of n = 5 experiments; *$p < 0.05$ and **$p < 0.01$ show significant differences compared to vehicle control.

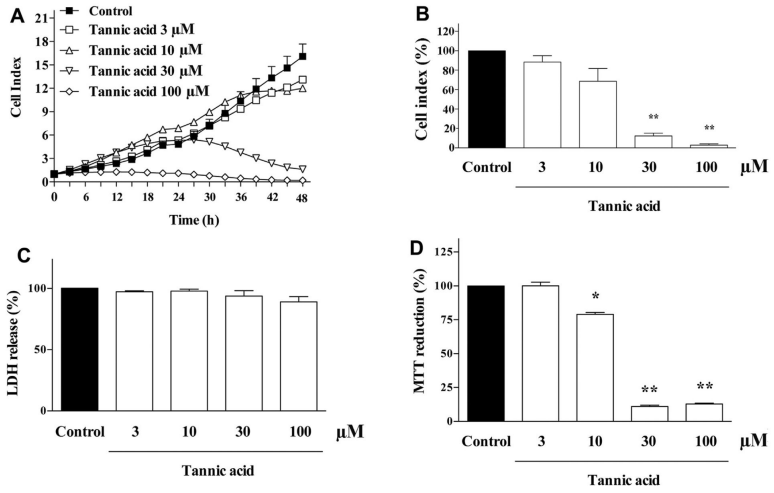


**Fig. 7.**

Effect of tannic acid (3 µM, 10 µM, 30 µM, 100 µM) on HCT116 cell proliferation and viability. (A): time-course of Cell Index, shown in a representative experiment; (B): summary data of Cell Index at 48 h; vehicle control values are normalized as 100%; (C): LDH release data at 48 h; vehicle control values are normalized as 100%; (D): MTT conversion data; vehicle control values are normalized as 100%. Data shown represent mean ± SEM of n = 5 experiments; *p < 0.05 and **p < 0.01 show significant differences compared to vehicle control.

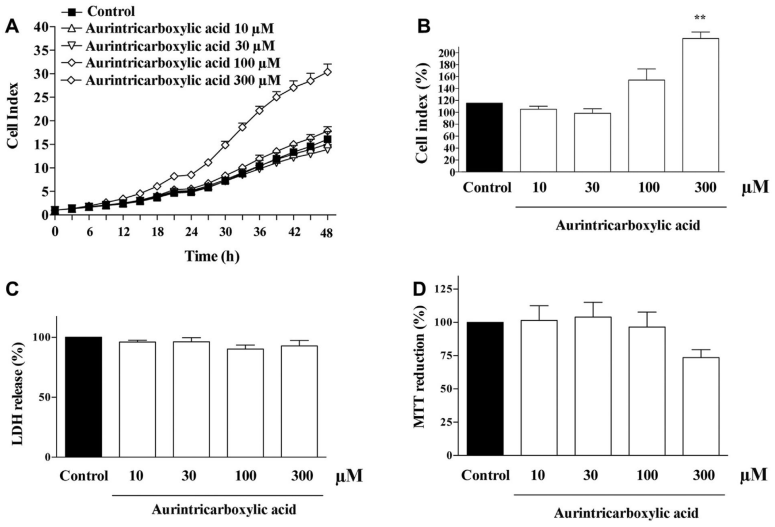


**Fig. 8.**

Effect of aurintricarboxylic acid (10 μM, 30 μM, 100 μM, 300 μM) on HCT116 cell proliferation and viability. (A): time-course of Cell Index, shown in a representative experiment; (B): summary data of Cell Index at 48 h; vehicle control values are normalized as 100%; (C): LDH release data at 48 h; vehicle control values are normalized as 100%; (D): MTT conversion data; vehicle control values are normalized as 100%. Data shown represent mean ± SEM of n = 5 experiments; **$p < 0.01$ shows significant differences compared to vehicle control.

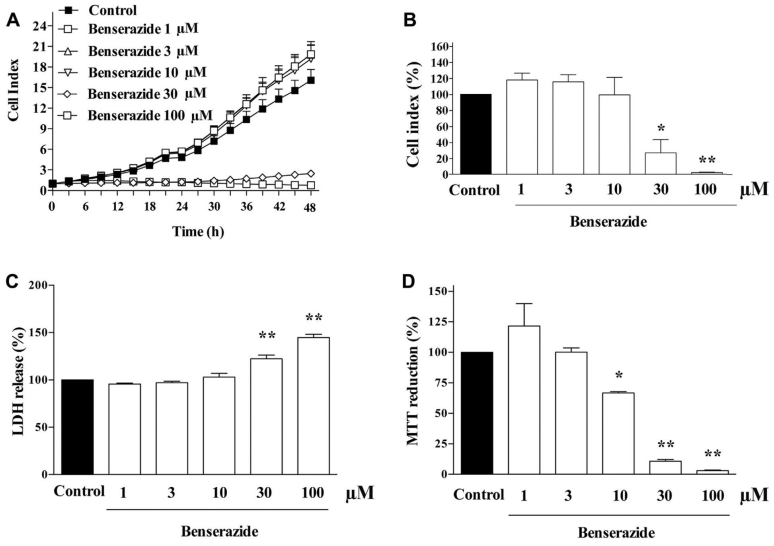


**Fig. 9.**

Effect of benserazide (1 μM, 3 μM, 10 μM, 30 μM) on HCT116 cell proliferation and viability. (A): time-course of Cell Index, shown in a representative experiment; (B): summary data of Cell Index at 48 h; vehicle control values are normalized as 100%; (C): LDH release data at 48 h; vehicle control values are normalized as 100%; (D): MTT conversion data; vehicle control values are normalized as 100%. Data shown represent mean ± SEM of n = 5 experiments; *p < 0.05 and **p < 0.01 show significant differences compared to vehicle control.

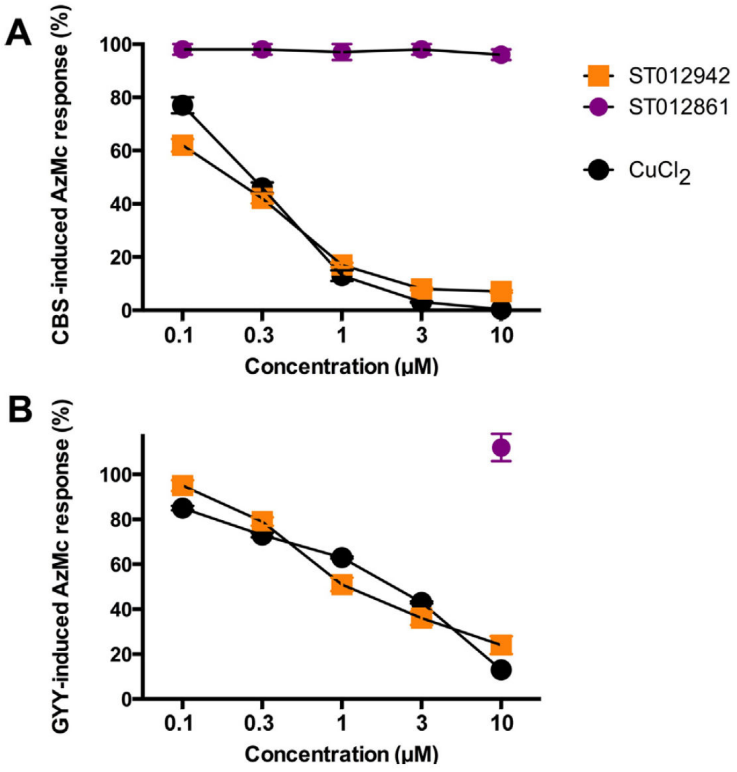


**Fig. 10.**

Effect of ST012861 (0.1 μM–10 μM), its copper-free analogue ST012942 and $CuCl_2$ (0.1 μM–10 μM) on (A) CBS-induced AzMC fluorescence and (B) GYY4187-induced AzMC fluorescence. Data represent mean values of triplicate determinations; Where SEM values are not shown, they are contained within the symbols.

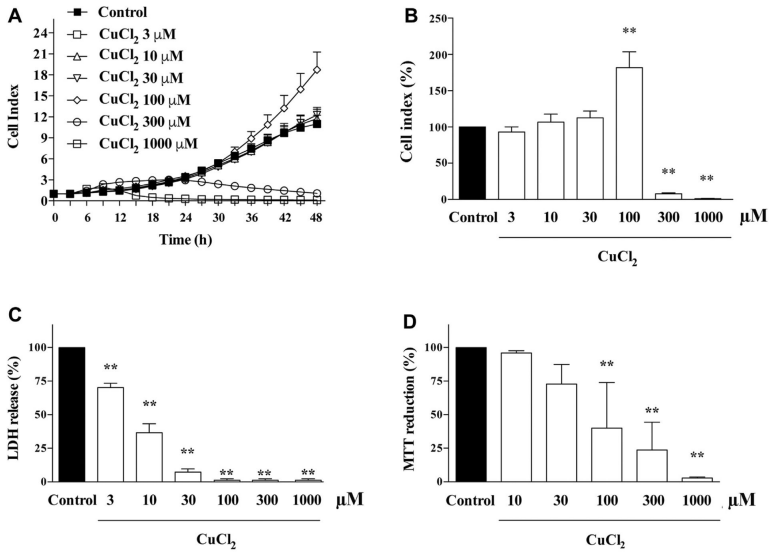


**Fig. 11.**

Effect of $CuCl_2$ (3 μM, 10 μM, 30 μM, 100 μM, 300 μM, 1 mM) on HCT116 cell proliferation and viability. (A): time-course of Cell Index, shown in a representative experiment; (B): summary data of Cell Index at 48 h; vehicle control values are normalized as 100%; (C): LDH release data at 48 h; vehicle control values are normalized as 100%; (D): MTT conversion data; vehicle control values are normalized as 100%. Data shown represent mean ± SEM of n = 3 experiments; *$p < 0.05$ and **$p < 0.01$ show significant differences compared to vehicle control.

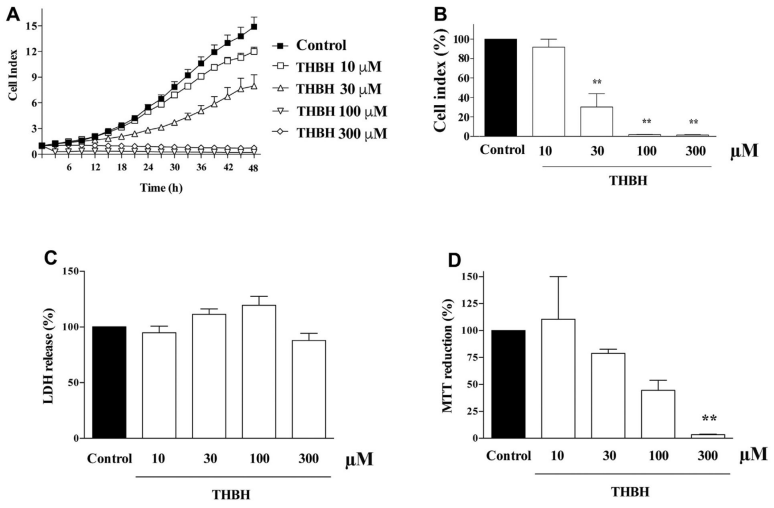


**Fig. 12.**

Effect of 2,3,4-trihydroxybenzylhydrazine (10 μM, 30 μM, 100 μM, 300 μM) on HCT116 cell proliferation and viability. (A): time-course of Cell Index, shown in a representative experiment; (B): summary data of Cell Index at 48 h; vehicle control values are normalized as 100%; (C): LDH release data at 48 h; vehicle control values are normalized as 100%; (D): MTT conversion data; vehicle control values are normalized as 100%. Data shown represent mean ± SEM of n = 5 experiments; **p < 0.01 shows significant differences compared to vehicle control.

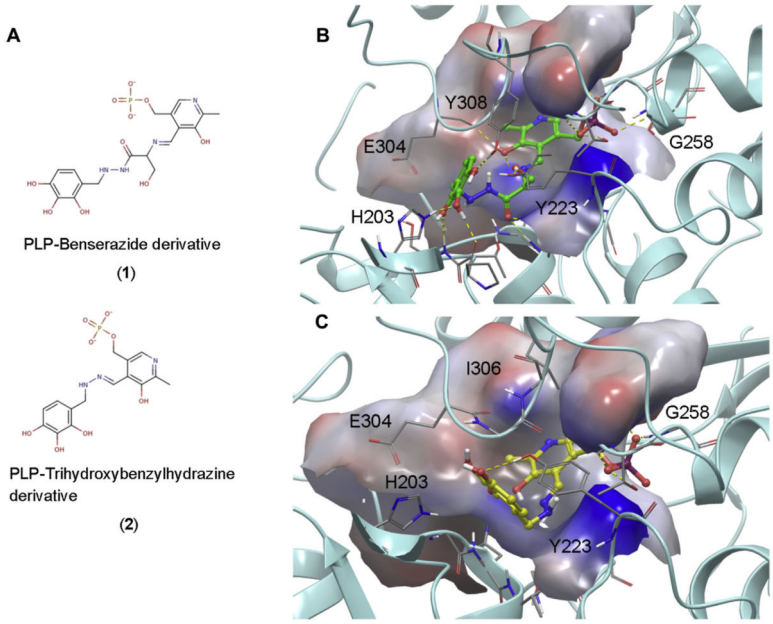


**Fig. 13.**

(A) The two potential derivatives of the reaction between PLP and either the unmodified benserazide (**1**) or the benserazide metabolite 2,3,4-trimethylbenzylhydrazine (**2**). (B) Proposed binding mode of derivative **1** (shown as a ball and stick model with green carbons) in the PLP binding cavity of CBS shown in a ribbon representation and an electrostatic potential-colored surface. A number of residues involved in binding are depicted in a stick representation while hydrogen bonds with residues of the PLP cavity periphery are shown as yellow dashed lines. (C) Proposed binding mode of derivative **2** (shown in a ball and stick representation with yellow carbons). (For interpretation of the references to colour in this figure legend, the reader is referred to the web version of this article.)

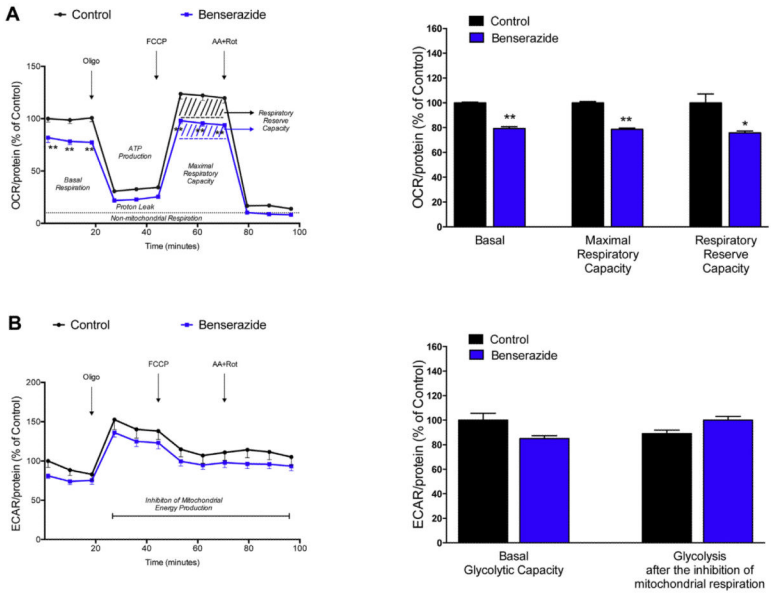


**Fig. 14.**

Effect of benserazide (10 μM) on the cellular bioenergetics of HCT116 cells. Parameters of (A) oxidative phosphorylation and (B) glycolysis are shown. Bioenergetic parameters were normalized to protein content. Data represent mean ± SEM of n = 5 determinations; *p < 0.05, **p < 0.01 show significant differences compared to vehicle control. show significant differences compared to vehicle control show significant differences compared to vehicle control.

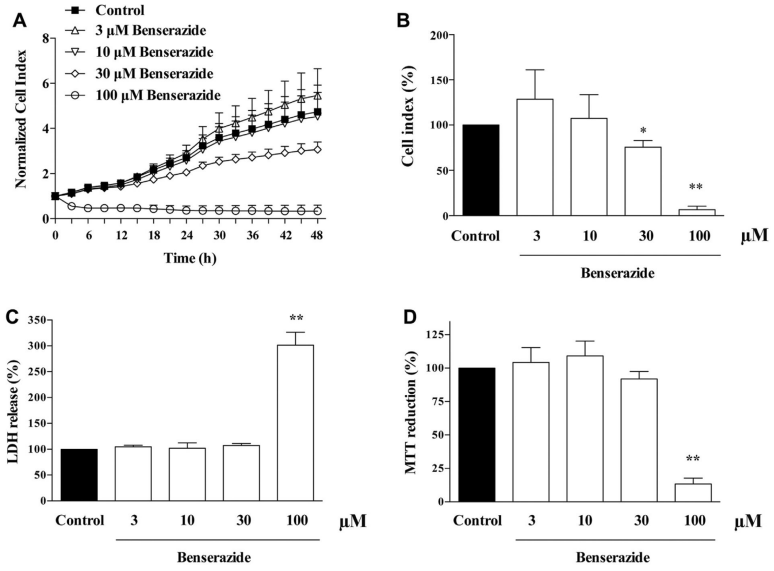


**Fig. 15.**

Effect of benserazide (3 μM, 10 μM, 30 μM, 100 μM) on HT29 cell proliferation and viability. (A): time-course of Cell Index, shown in a representative experiment; (B): summary data of Cell Index at 48 h; vehicle control values are normalized as 100%; (C): LDH release data at 48 h; vehicle control values are normalized as 100%; (D): MTT conversion data; vehicle control values are normalized as 100%. Data shown represent mean ± SEM of n = 3 experiments; *p < 0.05 and **p < 0.01 show significant differences compared to vehicle control.

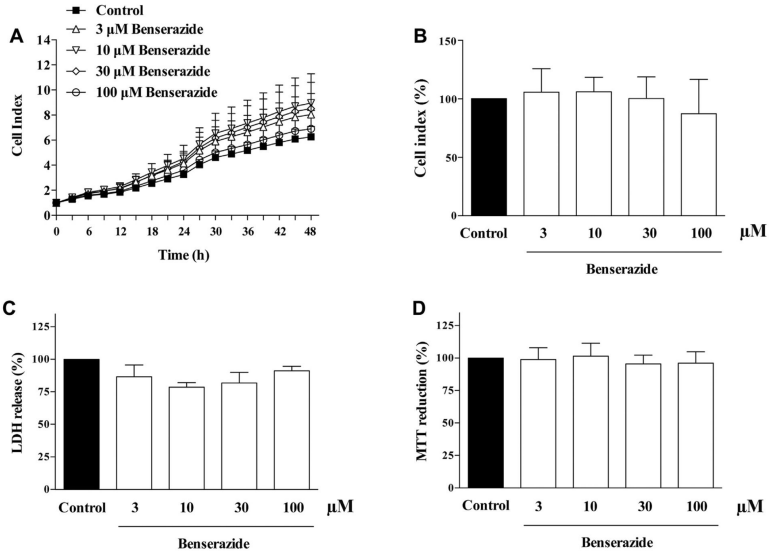


**Fig. 16.**

Effect of benserazide (3 μM, 10 μM, 30 μM, 100 μM) on LoVo cell proliferation and viability. (A): time-course of Cell Index, shown in a representative experiment; (B): summary data of Cell Index at 48 h; vehicle control values are normalized as 100%; (C): LDH release data at 48 h; vehicle control values are normalized as 100%; (D): MTT conversion data; vehicle control values are normalized as 100%. Data shown represent mean ± SEM of n = 3 experiments.

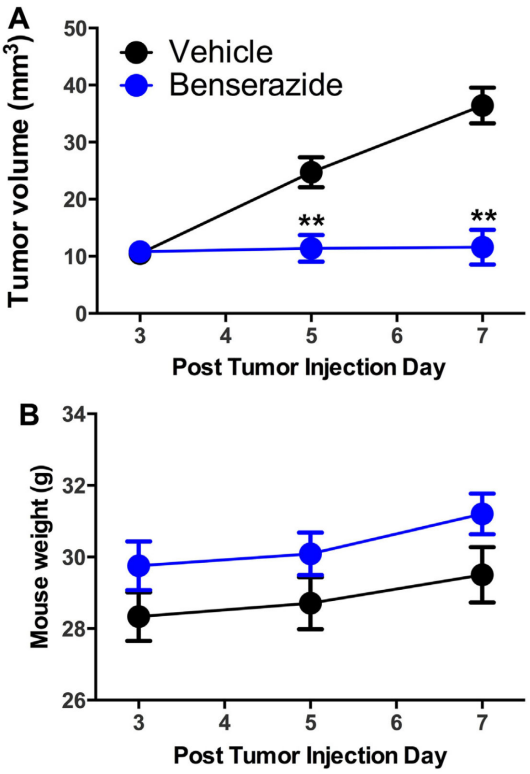


**Fig. 17.**

Effect of benserazide (50 mg/kg/day s.q.) on the growth of HT29 cell xenografts in nude mice. Data show mean ± SEM tumor sizes and animal weights of n = 9 mice per group. **p < 0.01 shows a significant effect of benserazide on tumor size compared to vehicle control.

## Table 1

List of libraries used for the current screening campaign.

| Library | Supplier | Description | Code | Number of compounds |
|---|---|---|---|---|
| LOPAC 1280 | Sigma-Aldrich Saint Louis, MO | Various biologically active compounds | LOPAC | 1280 |
| FDA Approved Library | Enzo Life Sciences Farmingdale, NY | FDA approved bioactive compounds | FDA | 640 |
| International Drug Collection | MicroSource Discovery Systems Gaylordsville, CT | Marketed in Europe or Asia but not in the US | IDC | 240 |
| Killer Plates | MicroSource Discovery Systems Gaylordsville, CT | Toxic substances | Killer | 160 |
| NIH Clinical Collection | BioFocus South San Francisco, CA | Phase I–III trial compounds | NIH | 446 |
| Prestwick Chemicals | Prestwick Chemicals Washington, DC | Marketed drugs in Europe | Prestwick | 1200 |
| TocriScreen | Tocris BioScience Ellsville, MI | Various biologically active compounds | Tocris | 1120 |
| US Drug Collection | MicroSource Discovery Systems Gaylordsville, CT | Clinical trial stage USA drugs | US Drug | 1040 |
| NPL-640 | Sigma-Aldrich Saint Louis, MO | Natural products | NP | 640 |
| ActiTarg P | TimTec LLC Newark, DE | Proteinase inhibitors | PI | 1140 |
| ActiTarg K | TimTec LLC Newark, DE | Kinase modulators | KM | 960 |
| PLP Custom | Sigma Aldrich | Known inhibitors of PLP-dependent enzymes | PLP | 5 |

## Table 2

List of potential hit compounds identified by the primary screening, and effect of the same compounds on GYY4137-induced fluorescence responses. Compounds were screened at 30 μM (except for compounds indicated by asterisk, where testing was conducted at the indicated concentration) against CBS-induced AzMC fluorescence and re-tested at 30 μM (except for compounds indicated by asterisk, where testing was conducted at the indicated concentration) against CBS- and GYY4137-induced AzMC fluorescence. Data are shown as mean ± SEM, n = 3.

| Potential hit compound | Library | Initial screen (% inhibition of CBS-induced AzMC fluorescence) | Confirmation (% inhibition of CBS-induced AzMC fluorescence) | Confirmation (% inhibition of GYY4137-induced AzMC fluorescence) |
|---|---|---|---|---|
| 5-(*N,N*-hexamethylene)amiloride | LOPAC | 72% | 58 ± 3 | 54 ± 4 |
| Ruthenium red | LOPAC | 72% | 72 ± 6 | 72 ± 3 |
| NSC 95397 (2,3bis[(2-Hydroxyethyl)thio]-1,4-naphthoquinone) | LOPAC | 70% | 59 ± 8 | 58 ± 1 |
| *O*-(Carboxymethyl)hydroxylamine hemihydrochloride (AOAA) | LOPAC | 70% | 89 ± 1 | 2 ± 1 |
| Aurintricarboxylic acid | LOPAC | 59% | 87 ± 1 | −2 ± 1 |
| Benserazide hydrochloride | LOPAC | 49% | 44 ± 1 | 4 ± 2 |
| Tyrphostin AG 537 | LOPAC | 49% | 42 ± 1 | 48 ± 2 |
| 2,3-Dimethoxy-1,4-naphthoquinone | LOPAC | 49% | 53 ± 1 | 51 ± 4 |
| Closantel | FDA | 43% | 25 ± 5 | 31 ± 2 |
| Progesterone | IDC | 68% | 75 ± 3 | 64 ± 1 |
| Nifuroxazide | IDC | 48% | 55 ± 4 | 50 ± 2 |
| Chlorophyllide cu complex Na salt | Killer | 82% | 97 ± 1 | 78 ± 3 |
| Juglone | Killer | 74% | 85 ± 1 | 61 ± 3 |
| Tannic acid | Killer | 73% | 43 ± 1 | 3 ± 2 |
| 4,4′-diisothiocyanostilbene-2,2′-sufonic acid sodium salt (DIDS) | Killer | 69% | 58 ± 4 | 56 ± 5 |
| Phenylmercuric acetate | Killer | 69% | 50 ± 6 | 59 ± 2 |
| Verteporfin | Prestwick | 69% | 41 ± 5 | 38 ± 5 |
| Clofazimine | Prestwick | 47% | 30 ± 7 | 28 ± 5 |
| NSC 95397 (2,3bis[(2-Hydroxyethyl)thio]-1,4-naphthoquinone) | Tocris | 68% | 58 ± 8 | 58 ± 1 |
| NSC 3852 (5-Nitroso-8-quinolinol) | Tocris | 58% | 48 ± 5 | 47 ± 5 |
| Ro-08-2750 (2,3,4,10-Tetrahydro-7,10-dimethyl-2,4-dioxobenzo[*g*]pteridine-8-carboxaldehyde) | Tocris | 55% | 59 ± 3 | 69 ± 8 |
| Chlorophyllide Cu complex Na salt | US Drugs | 80% | 97 ± 1 | 78 ± 3 |
| Tannic acid | US Drugs | 73% | 43 ± 1 | 3 ± 2 |
| Phenylmercuric acetate | US Drugs | 52% | 29 ± 4 | 32 ± 4 |
| Nitrofurazone | US Drugs | 52% | 54 ± 2 | 48 ± 5 |
| Pyrvinium pamoate | US Drugs | 49% | 468 ± 1 | 36 ± 3 |
| Hexachlorophene | US Drugs | 48% | 12 ± 1 | 1 ± 1 |
| ST012942* | NPL-640 | 86% (15 μM) | 96 ± 1 (15 μM) | 79 ± 2 (15 μM) |
| Dehydroglaucine* | NPL-640 | 62% (17 μM) | 82 ± 4 (17 μM) | 57 ± 8 (17 μM) |

| Potential hit compound | Library | Initial screen (% inhibition of CBS-induced AzMC fluorescence) | Confirmation (% inhibition of CBS-induced AzMC fluorescence) | Confirmation (% inhibition of GYY4137-induced AzMC fluorescence) |
|---|---|---|---|---|
| Gossypolone* | NPL-640 | 57% (12 μM) | 30 ± 5 (12 μM) | 25 ± 4 (12 μM) |

## Table 3

Effect of AOAA, NSC67078, hexachlorophene, aurintricarboxylic acid, tannic acid and benserazide (10, 30 and 100 μM) on CBS- and GYY4137 induced $H_2S$/AzMC fluorescence responses and CBS-induced methylene blue $H_2S$ responses. Data are shown as mean ± SEM of n = 3 separate determinations.

| Compound | % inhibition of CBS –induced AzMC fluorescence | % inhibition of CBS –induced methylene blue signal | % inhibition of GYY4137 –induced AzMC fluorescence |
|---|---|---|---|
| AOAA (10 μM) | 80 ± 1 | 49 ± 3 | 3 ± 2 |
| AOAA (30 μM) | 89 ± 1 | 67 ± 1 | 2 ± 1 |
| AOAA (100 μM) | 94 ± 1 | 76 ± 1 | 1 ± 1 |
| NSC67078 (1 μM) | 47 ± 1 | 59 ± 2 | 25 ± 1 |
| NSC67078 (10 μM) | 88 ± 1 | 73 ± 1 | 65 ± 1 |
| NSC67078 (30 μM) | 93 ± 1 | 95 ± 1 | 78 ± 1 |
| Hexachlorophene (10 μM) | 3 ± 1 | 21 ± 1 | −4 ± 2 |
| Hexachlorophene (30 μM) | 12 ± 1 | 31 ± 1 | 1 ± 3 |
| Hexachlorophene (100 μM) | 70 ± 1 | 64 ± 1 | −2 ± 1 |
| Aurintricarboxylic acid (10 μM) | 72 ± 1 | 38 ± 2 | −3 ± 2 |
| Aurintricarboxylic acid (30 μM) | 87 ± 1 | 61 ± 1 | −2 ± 1 |
| Aurintricarboxylic acid (100 μM) | 94 ± 1 | 72 ± 1 | 6 ± 1 |
| Tannicacid (10 μM) | 28 ± 2 | 24 ± 9 | −1 ± 1 |
| Tannic acid (30 μM) | 43 ± 1 | 46 ± 3 | 3 ± 2 |
| Tannic acid (100 μM) | 75 ± 1 | 56 ± 3 | 8 ± 3 |
| Benserazide (10 μM) | 29 ± 1 | 24 ± 5 | 2 ± 2 |
| Benserazide (30 μM) | 44 ± 1 | 33 ± 3 | 4 ± 2 |
| Benserazide (100 μM) | 66 ± 1 | 50 ± 2 | 1 ± 1 |

**Table 4**

Effect of three copper compounds on CBS- and GYY4137-induced $H_2S$/AzMC fluorescence responses. Data are shown as mean ± SEM of n = 3 separate determinations.

| Compound | % inhibition of CBS–induced AzMC fluorescence | % inhibition of GYY4137–induced AzMC fluorescence |
|---|---|---|
| $CuCl_2$ (0.1 μM) | 36 ± 1 | 1 ± 1 |
| $CuCl_2$ (0.3 μM) | 60 ± 2 | 10 ± 1 |
| $CuCl_2$ (1 μM) | 90 ± 1 | 14 ± 1 |
| CuAc (0.1 μM) | 39 ± 1 | 2 ± 2 |
| CuAc (0.3 μM) | 66 ± 1 | 12 ± 1 |
| CuAc (1 μM) | 92 ± 1 | 17 ± 1 |
| $Cu(NO_2)_2$ (0.1 μM) | 42 ± 1 | 5 ± 1 |
| $Cu(NO_2)_2$ (0.3 μM) | 70 ± 1 | 9 ± 13 |
| $Cu(NO_2)_2$ (1 μM) | 93 ± 2 | 16 ± 13 |